# Optical Oxygen Sensing Based on Ruthenium and Porphyrin Complexes

By
Daragh Dowling B.Sc. (Hons)

A Thesis Presented
to
Dublin City University

Submitted for the Degree of Master of Science

Research Supervisor
Dr. Colette McDonagh,
School of Physical Sciences,
Dublin City University.

April 2002

## Declaration

I hereby certify that this material, which I now submit for assessment on the programme of study leading to the award of Master of Science, is entirely my own work and has not been taken from the work of others, save, and to the extent, that such work has been cited and acknowledged during the text of my work.

Signed: _____ Date: _____

# Acknowledgements

To Colette, for all her guidance, support and help during my time at DCU, both during my undergraduate degree and especially during my time in the Optical Sensors Laboratory. Her continuous encouragement and ideas were ceaseless and informative. Thanks also for the affording me opportunity to 'sabbatical' in New Zealand.

Thanks to Brian, for his tremendous support of this project, despite his overwhelming commitments elsewhere. His enthusiasm for scientific research was a breath of fresh air, even during the most frustrating of times.

To everyone at the OSL, both past and present, thanks for all the good times and fun we had. For the countless coffee breaks, the games of soccer and the nights out on the tiles. I've enjoyed every minute of it. A special mention must go to Aisling, my fellow oxygen researcher. Thanks for all your help, motivation and friendship over the last 3 years.

I would like to thank and acknowledge everyone in the Physics Department of DCU for all their help and advice, especially Tony Cafolla for his programming expertise, and Des Lavelle for producing excellent pieces of equipment at very short notice.

To my friends and family, I owe a great debt of gratitude. Their tireless companionship and kindness was (and hopefully will remain) a source of great encouragement. To the lads, Dave, Simon, Brian, and everyone else at Suttonians RFC, thanks for providing an enjoyable distraction from DCU (although some might say that DCU did the opposite!).

To Caroline - finally a mention! Thanks for all your support, patience and above all friendship. You always had a spare ear to listen to my grumblings, and a kind word to pick me up when I was down. The interest you took in the 'sick probe' was inspiring and helped me to keep the faith.

To my sister and brother, Aoife and Finbar, you'll have to find somewhere else to print out assignments now! Thanks for making the car journeys both enjoyable and interesting.

Finally to my parents, Jim and Cepta, to whom I am dedicating this thesis. Through their help, support and interest they made this achievement possible. I only hope that someday I can begin to pay them back for everything that they have done for me.

# Dedication

To Jim and Cepta

# Abstract

The design and performance of a ruggedised dissolved oxygen probe, both in the laboratory and in the field, are reported. This probe is based on phase fluorometric detection of the quenched fluorescence of an oxygen-sensitive ruthenium complex. Dissolved oxygen probes have a number of different applications e.g. in bioreactors, in living systems, in industry and in waste-water treatment plants. The probe reported here has been developed specifically for waste-water monitoring. The oxygen-sensitive complex is entrapped in a porous hydrophobic sol-gel matrix that has been optimised for this application. Light emitting diode (LED) excitation and photodiode detection are employed in a dipstick probe configuration, with the oxygen-sensitive film coated on a disposable Poly(methyl methacrylate)(PMMA) disc, which in turn is designed to optimise guiding of the excitation light into the film. A key element of the design is the common mode rejection of phase between the signal and reference channels, requiring careful selection of the relevant opto-electronic components.

Extensive laboratory testing has been carried out on this sensor, and it exhibited high performance with limit of detection typically 6 ppb, sensor resolution of 15 ppb at 9 ppm oxygen concentration, and excellent long term stability of 0.1 ppm per week. A first phase of field testing at a UK waste-water treatment plant has taken place and a second is planned for 2002.

Also reported here is the optimisation of films, which have Platinum Octoethyl-porphyrin keytone (PtOEPk) entrapped as the oxygen-sensitive complex. The fluorescence from the PtOEPk is quenched in the presence of oxygen, in a similar way to the ruthenium complex. The longer lifetime of PtOEPk allows for greater sensitivity at lower oxygen concentrations. Several different support matrices for the porphyrin have been investigated using a fibre optic sensor, optimised for working with PtOEPk.

# Contents

# Chapter 1

# Introduction

## 1.1 Environmental Sensing: The Importance of Oxygen

The vital importance of oxygen for the sustainment of life, coupled with its mass involvement in natural processes and its widespread use in many working environments, has prompted much research. Of growing importance, worldwide, is the ability to accurately determine oxygen concentrations. Many applications, including medical, industrial, and environmental-sensing, rely heavily on the accurate measurement of oxygen, both in its gaseous and dissolved states[?, ?]. Of particular importance, and relevance to the work reported here, is dissolved oxygen (DO).

All naturally occurring water contains some dissolved contaminants, whether they are gases or salts. Water in its purest, non-contaminated form, does not exist outside of a laboratory environment. The level of oxygen dissolved in water can be taken as an indicator of the quality of the water. The careful and continuous control and monitoring of these levels of DO is of major importance in fermentation processes, and food preparation. The continuous in-situ monitoring of oxygen levels, by optical methods, is the main aim of this research work.

## 1.2 Optical Oxygen Sensing

A sensor is a device that produces a signal, or change in signal, due to a change in a physical parameter, or the presence of a particular analyte. Optical sensors produce a change in optical signal which can be described as a function of the measurand.

This optical signal can be an absorbance or fluorescence signal. Optical sensors are advantageous due to their ease of use, their cost effectiveness, the wide availability of inexpensive optoelectronic components (LEDs, photodiodes), and the ease with which they can be miniaturized to suit particular applications. Also advantageous is the fact that optical signals do not suffer from electrical interference.

Optical oxygen sensors, in particular, have many advantages over their electrochemical counterparts, for example, the amperometric Clark electrode[1]. Optical DO sensors have fast response times, are not easily poisoned, do not consume oxygen during the measurement process, and do not require stirring of the water to achieve an accurate measurement.

The most widely used method of optical oxygen sensing is based on collisional quenching of fluorescence from a fluorophore, in the presence of molecular oxygen. Much research has been done in this laboratory[2, 3, 4] on optical oxygen sensors based on the collisional quenching of an oxygen-sensitive complex. The details of the quenching process are described in Section 2.5.

## 1.3 Context of Research Work

As mentioned in Section 1.1, the monitoring of DO levels in-situ is an increasingly important process. This is most evident in the waste-water management industry. Continuous monitoring of DO levels on site at a waste-water treatment plant allows waste-water management companies to reliably and efficiently control the oxygen levels present in their water tanks.

The introduction of oxygen to water tanks in waste-water plants is one of the more basic, yet most efficient ways of treating waste-water. The presence of oxygen assists in the breakdown of biomass contained in the waste-water. However introducing too much oxygen in a treatment plant can be wasteful and can increase operating costs, making the entire process inefficient. By knowing the amount of oxygen that is introduced into the waste-water, and monitoring the level of DO that remains, waste-water management companies can reliably tell the quality of the water, and regulate the supply of oxygen accordingly. If the water is of a sufficiently high quality it can be released back into the natural waterways. However if it is not, it can be further treated, while being constantly monitored, until such a time as it is deemed fit to rejoin the natural waterway system[?].

A large part of this project involved testing an optical oxygen probe based on

fluorescence decay-time quenching of a Ruthenium complex:

$$Ru(II)tris(4,7-diphenyl-1,10-phenanthroline) \quad or \quad [Ru(Ph_2phen)_3]^{2+}$$

which was entrapped in a sol-gel thin film. The probe had been developed in house to meet the specifications of the waste-water industry. Chapter 5 of this thesis reports the work involved in the optimisation and testing of the prototype probe. The results of preliminary field tests are also reported.

Another oxygen-sensitive complex was also investigated during the course of this work. Platinum Octoethylporphyrin keytone (PtOEPk), a metallo-porphyrin, was investigated due to its high oxygen sensitivity at low oxygen levels. This work was carried out partly to address the fact that the levels of DO encountered in waste-water are normally very small, and their rates of change even smaller. Having a complex that is highly sensitive in this low level area is advantageous, as the accuracy and precision of oxygen measurements can be greatly improved.

Several support matrices for PtOEPk were investigated and some initial testing was done in a laboratory environment, initially in gas phase . Comparisons between Ru and PtOEPk were made and a number of different sensor configurations and instrumentations were employed. These results, along with suggestions for further work in this area, are presented in Chapters 6, 7 and 8.

## 1.4 Objectives of the Project

1. To optimise and test a prototype dissolved oxygen sensor.
2. To initiate field testing and make appropriate modifications/improvements.
3. To test and characterise a commercial porphyrin-based oxygen sensor and to investigate the use of porphyrin complexes in oxygen sensing, in particular to fabricate and evaluate porphyrin-doped sol-gel films.
4. To test a newly-designed modular phase-fluorometric system using both ruthenium complex-doped and porphyrin-doped films.

# Bibliography

[1] L.C. Clarke Jr. Monitor and control of blood and tissue oxygen tensions. *Trans. Amer. Artif. Intern. Organs*, 2:41, 1956.

[2] B. MacCraith, G. O'Keeffe, A.K. McEvoy, C.M. McDonagh, J.F. McGilp, B. O'Kelly, J.D. O'Mahony, and M. Cavanagh. Light-eitting-diode-based oxygen sensing using evanescent wave excitation of a dye-doped sol-gel coating. *Optical Engineering*, 33(12):3861–3866, 1994.

[3] B. MacCraith, C.M. McDonagh, G. O'Keeffe, E.T. Keyes, J.G. Vos, B. O'Kelly, and J.F. McGilp. Fibre optic oxygen sensor based on fluorescence quenching of evanescent-wave excited ruthenium complexes in sol-gel derived porous coatings. *Analyst*, 118:385–388, 1993.

[4] G. O'Keeffe, B.D. MacCraith, A.K. McEvoy, C.M. McDonagh, and J.F. McGilp. Development of a led-based phase-fluorimetric oxygen sensor using evanescent wave excitation of a sol-gel immobilized dye. *Sens and Act B*, 29:226–230, 1995.

# Chapter 2

# Oxygen Sensing by Fluorescence Quenching

## 2.1 Introduction

Optical sensors have been developed to measure a wide variety of different analytes. In the Optical Sensors Laboratory (OSL) at Dublin City University (DCU) researchers have developed sensors for ammonia, pH, carbon dioxide ($CO_2$) and oxygen, among others, using optical methods[1, 2, 3]. In recent years optical oxygen sensors based on fluorescence quenching have been developed for a wide range of applications[4, 5].

Fluorescence involves a fluorophore being optically excited at a particular wavelength (light emitting diodes(LEDs)[2] are commonly used as excitation sources due to the wide range of low cost LEDs available at many different wavelengths). The excited fluorophore then fluoresces. It is this emitted light that is quenched, or reduced, in the presence of the analyte and detected, usually using a photodiode (PD).

Whether in a gaseous state or dissolved in an aqueous solution, the amount of fluorescence measured is reduced as the oxygen concentration increases. As discussed in the following sections, the oxygen dependent optical signal can be measured by monitoring either fluorescence intensity or fluorescence decay time.

## 2.2 Fluorescence and Fluorescence Decay Time

In the work reported here, the presence and concentration of molecular oxygen is determined through the measurement of the fluorescence of a fluorophore, and in particular, the measurement of the optical decay time of this fluorescence. To fully understand this process it is vital to first of all understand the principles involved.

### 2.2.1 Fluorescence

Fluorescence refers to the emission of light from a fluorophore by means of some radiative decay process. Fluorescence occurs when electrons from the stable ground state are excited to a higher excited state and subsequently de-excite.

These excited electrons remain in the excited state until such a time as they can find a mechanism to return to the ground state. These mechanisms have been detailed extensively by Lakowicz [6]. They include both non-radiative and radiative decay processes. When an electron decays from an excited state radiatively, a photon of a specific wavelength is emitted. It is this emitted light that is termed fluorescence. A simplified diagram that explains this process is shown in Figure 2.1.

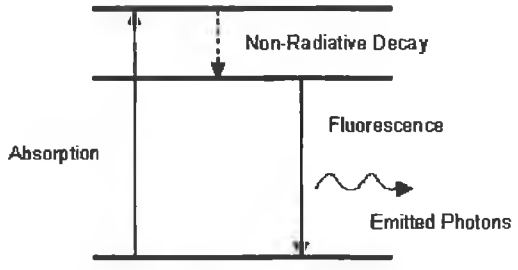


**Figure 2.1: Shows the mechanisms by which Fluorescence occurs.**

In most fluorescing materials the fluorescence occurs at a higher wavelength (lower energy) than the absorption. This is called the Stokes shift[6, 7]. A large Stokes shift is desirable, as discussed later in this chapter.

### 2.2.2 Fluorescence Decay Time

It is not only the intensity of the fluorescence of the indicator dyes that is reduced in the presence of molecular oxygen, but also its fluorescence decay time. The fluorescence decay time of a fluorophore is an intrinsic property of the fluorophore. A typical decay time measurement is shown in Figure 2.2. The decay time ($\tau$) is

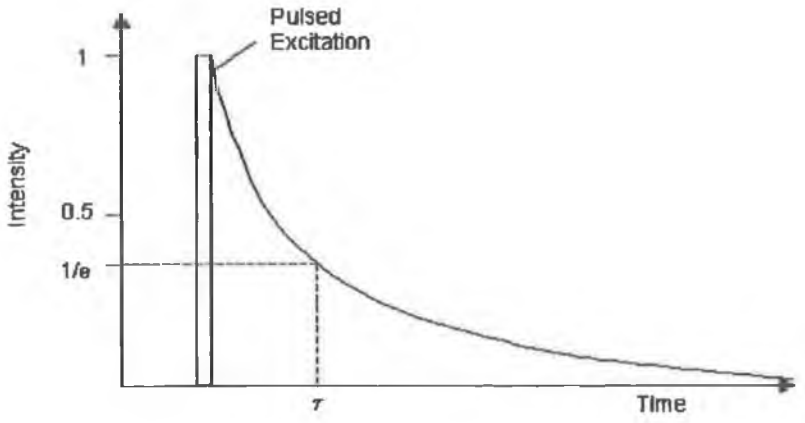


**Figure 2.2:** Typical decay time fall off after pulsed excitation.

taken as the time for the fluorescence to fall off to a value $1/e$ of its maximum, if the decay is single exponential. Some of the advantages of measuring changes in $\tau$, compared with changes in the intensity, are that it is virtually independent of signal drift caused by aging optoelectronic components, and also independent of the amount of stray light in the system[8]. The fluorescence decay time or lifetime ($\tau$) can be defined as the average period of time a fluorescent molecule spends in the excited state before returning to the ground state. This observed decay time depends on non-radiative and radiative decay rates and is given by Equation 2.1

$$\kappa_{obs} = \frac{1}{\tau_{obs}} = \frac{1}{\tau_{rad}} + \frac{1}{\tau_{non-rad}} \tag{2.1}$$

where $\frac{1}{\tau}$ is equal to the decay rate, $\kappa$ and where obs., rad. and non-rad. refer to observed, radiative and non-radiative respectively. The lifetime method is used exclusively in this work.

As discussed later, the lifetimes obtained from glass sensor films are generally not single exponential.

## 2.3 Ruthenium Complexes

The fluorophore or fluorescent complex used for the detection of oxygen in the DO monitoring probe, which encompasses a large part of this work, was a ruthenium-based complex $[Ru(Ph_2phen)_3]^{2+}$. This transition metal complex has been used extensively in oxygen sensor development research carried out at this sensor laboratory[9] and worldwide[10]. Its popularity stems from its highly emissive metal-to-ligand charge-transfer state, its long lifetime, hence its large oxygen sensitivity, and its strong absorption in the blue-green region of the visible spectrum[11]. This complex, and ones similar to it in structure, are also popular due to their high thermal, chemical and physical stability, and also for the ease with which they can be incorporated into support matrices.

A diagram of the chemical structure of the complex is given in Figure 2.3. A detailed description of its chemical make-up and electronic structure is beyond the scope of this work but can be found in the Ph.D. thesis of McEvoy[12].

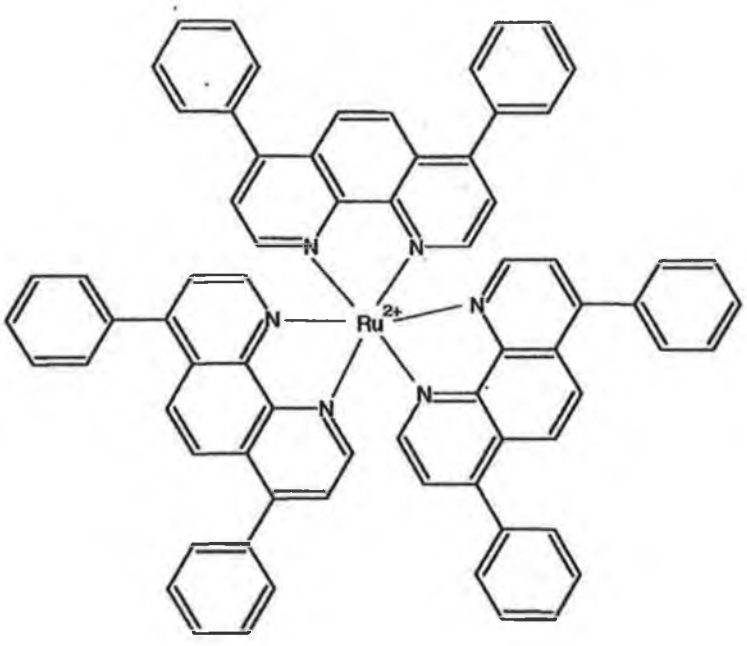


**Figure 2.3:** Ruthenium chemical structure.

The strong absorption band of the $[Ru(Ph_2phen)_3]^{2+}$ complex in the blue-green region of the visible spectrum allows for excitation of the fluorophore with widely available, inexpensive optoelectronic sources. Chosen for use in this work was a high

intensity blue LED, with a peak emission wavelength of 450nm. Upon excitation with this LED, the Stokes-shifted fluorescence of $[Ru(Ph_2phen)_3]^{2+}$ occurs with a peak wavelength of 608nm. This large Stokes shift allows for relatively easy filtering of the light at the PD detector.

Below (Figure 2.4) is a diagram showing the excellent overlap between the chosen excitation LED and the absorption band of $[Ru(Ph_2phen)_3]^{2+}$, along with the large Stokes-shifted fluorescence. This plot was generated using data measured using an Ocean Optics $\mu$-spectrometer.

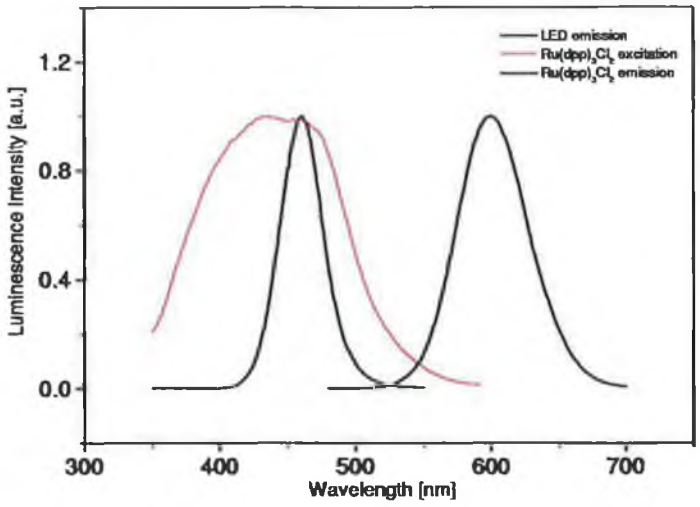


**Figure 2.4:** Overlap of $Ru^{2+}$ Excitation, Fluorescence and LED Emission.

## 2.4 Porphyrin Complexes

Recently there has been a great deal of research into alternative oxygen sensitive complexes, in particular metallo-porphyrins. These complexes generally have longer decay times than the $[Ru(Ph_2phen)_3]^{2+}$ complex. They are highly emissive with absorption bands at convenient wavelengths for available LEDs, and their emission in the near infra-red (IR) is easily detectable by photodiodes[13]. These complexes, while having a much greater oxygen sensitivity due to their longer $\tau$ (see Section 2.5), are less photostable[14]. Further research however has revealed that through the use of certain porphyrin ketones the photostability can be improved[15]. Recently

a porphyrin complex with increased photostability has been identified[16]. This complex is Platinum Octoethlyporphyrin ketone (PtOEPk) and it has been chosen for this work. This phosphorescent complex exhibits strong phosphorescence at room temperature, in the near infra-red region of the electromagnetic spectrum, and has a notably longer lifetime than that of the ruthenium complex discussed in the previous section.

These new porphyrin ketones possess absorption bands which correspond well with available optoelectronic excitation sources. Their excited state emission band occur at wavelengths that are compatible with widely available semiconductor photodiode detectors. The overlap of the excitation LED and the PtOEPk absorption, and emission bands, is shown in Figure 2.5, in a similar fashion to that for $[Ru(Ph_2phen)_3]^{2+}$ in Figure 2.4. Again the data used to generate this plot was measured using the same Ocean Optics $\mu$-spectrometer.

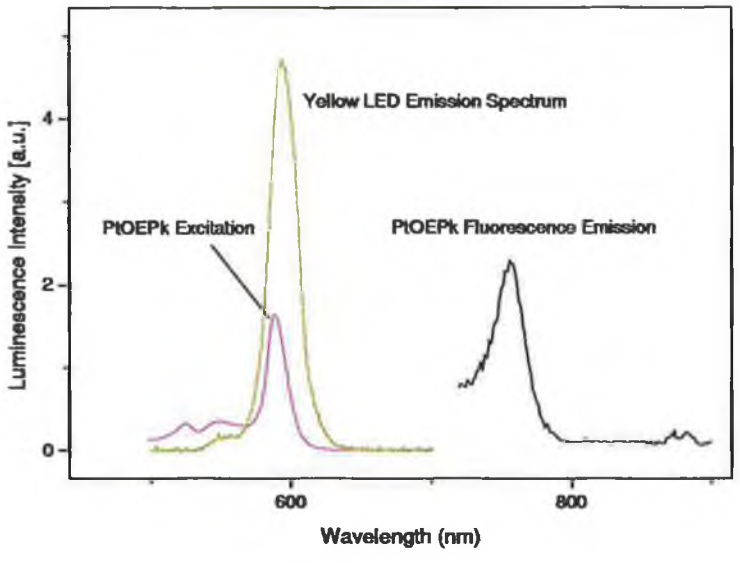


**Figure 2.5:** Overlap of PtOEPk Absorption and Emission Spectra, as well as Excitation LED.

## 2.5 Quenching by Oxygen of Fluorescence and Decay Times

Quenching of fluorescence refers to any process that reduces the fluorescence intensity of a given fluorophore [6]. When the fluorophore is in an excited state this can happen through one, or more different processes. These processes include non-radiative decay, excited state reactions, energy transfer within the complex and collisional quenching. It is this last process that is of importance in this work.

Oxygen is an excellent quencher of the fluorescence of many different fluorophores, and much research has been carried out on optical oxygen sensors[2, 3]. The quenching process is collisional quenching, which involves direct contact between the excited fluorophore and the quenching analyte, molecular oxygen in this case.

This so-called dynamic quenching is described by the Stern-Volmer equations[6, 7], Equations 2.2 and 2.3.

$$\frac{I_0}{I} = 1 + \mathrm{K}_{SV} pO_2 = 1 + k\tau_0[Q] \qquad (2.2)$$

$$\frac{\tau_0}{\tau} = 1 + \mathrm{K}_{SV} pO_2 = 1 + k\tau_0[Q] \qquad (2.3)$$

$$\mathrm{k} \propto \alpha \mathrm{D} \qquad (2.4)$$

where I is the fluorescence intensity, $\tau$ is the mean lifetime of the fluorescence, $\mathrm{K}_{SV}$ is the Stern-Volmer constant, $\mathrm{pO}_2$ is oxygen partial pressure, k is the bimolecular quenching constant, Q is the oxygen concentration and the subscript 0 denotes the absence of oxygen. In Equation 2.4, the bimolecular quenching constant, k, is related to the oxygen solubility, $\alpha$, in the support matrix and the diffusion coefficient in the

matrix, D. A plot of $\frac{I_0}{I}$ or $\frac{\tau_0}{\tau}$ as a function of oxygen partial pressure or oxygen concentration should yield a straight line of slope $K_{SV}$. This is shown in Figure 2.6. The data used in this plot was generated using Microcal Origin. It is to be noted that Stern-Volmer plots are often non-linear, due to the interaction between the oxygen diffusing into the sol-gel matrix and the fluorescent complex molecules entrapped in the matrix. This is discussed further in Chapter 6.

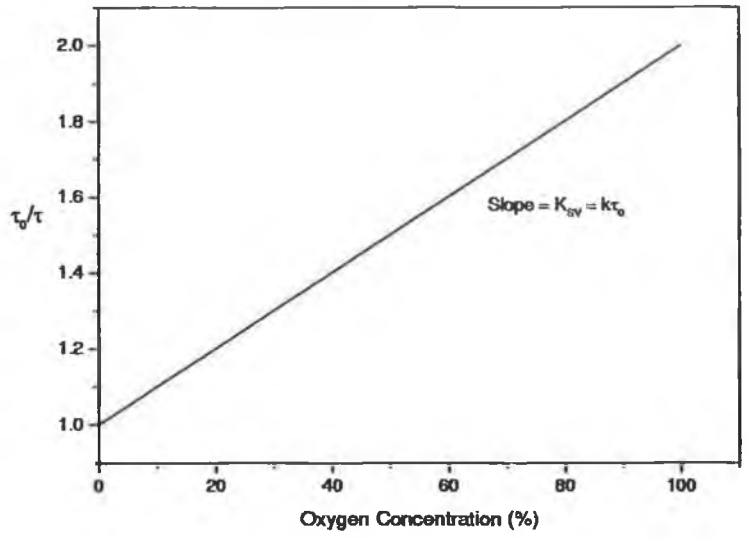


**Figure 2.6:** Linear/Ideal Stern-Volmer plot.

## 2.6 Phase-Fluorometric Detection

The oxygen-quenched fluorescence intensity is affected by base-line drift due to LED fluctuations and sensor positioning variations. Dye leaching and photobleaching can also alter the intensity. Leaching is a process whereby weakly bound dye molecules are washed out of the sensor film in an aqueous environment, while photobleaching is a complex process where the excitation source alters the dye photochemistry thereby reducing the emitted intensity[17]. Many of these problems, in particular the LED drift due to temperature changes, can be overcome by using a phase fluorometric approach which involves operating in the time domain according to Equation 2.3 instead of in the intensity domain. Measurements of fluorescence quenching by molecular oxygen can be made directly by exciting the sensor film with a pulse of

light and measuring the decay time (the time taken for the fluorescence to decay to a value $1/e$ of its maximum). This was shown in Figure 2.2.

Phase fluorimetry is a more indirect method of measuring in the time domain. Here the sensor film is excited by a light source sine-wave modulated at a particular frequency. The fluorescence output from the film is then modulated at the same frequency. By measuring the phase-shift between these two waveforms the oxygen concentration can be determined[2]. This is shown in Figure 2.7. This figure shows two generated sine waves out of phase that represent the signals detected by the photodiode. The technique used to achieve these phase-shift measurements is known as phase-fluorometric detection.

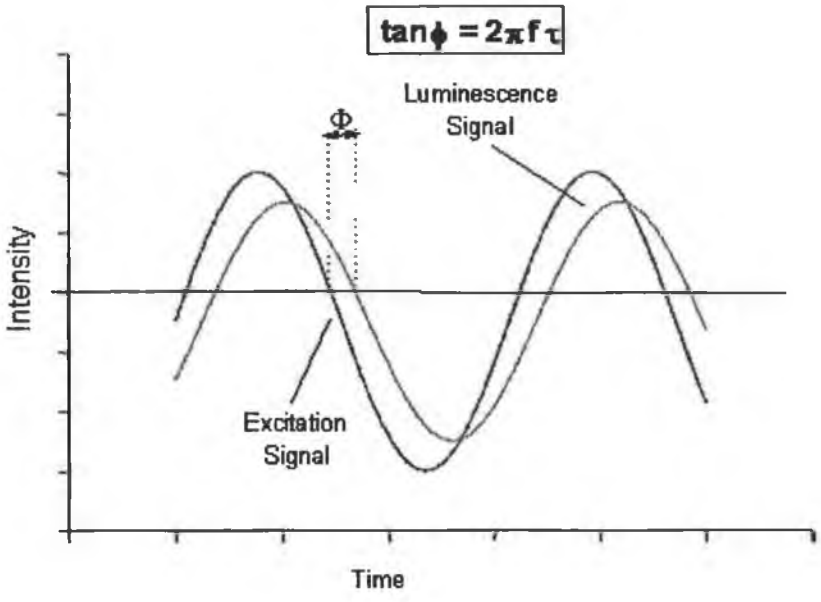


**Figure 2.7:** Sin-Wave Modulated Excitation Light with Resultant Fluorescence.

The phase-shift occurs due to the fact that the fluorescence waveform lags the excitation waveform by some amount, $\phi$. As shown by Equation 2.5 $\phi$ is related to the decay time of the fluorescence $\tau$, and hence has a dependence on the concentration of oxygen present in the sensor matrix. Here f is the modulation frequency.

$$\tau = \frac{\tan(\phi)}{2\pi \mathrm{f}} \tag{2.5}$$

The technique described above is that used in the experiments on both of the fluorophores investigated during the course of this work, although the instruments used were different.

## 2.7 Temperature Dependence of Quenching

Both the oxygen-sensitive fluorescence and the quenching process are sensitive to temperature. This section discusses the origin of this temperature dependence. Both sensor systems used throughout the course of the work contained the ability to record the external temperature, at a point as close as possible to the sensor film. These data could then used to compensate for any temperature changes that may have affected the sensor response.

There are two contributing factors to the temperature dependence, namely, the temperature dependence of the fluorescence intensity and that of the quenching response. The temperature dependence of the absolute fluorescence intensity is related to the change in quantum efficiency with temperature. This affects the lifetime and consequently the phase shift, $\phi$. A decrease in absolute fluorescence intensity occurs with increasing temperature. The quenching response is also temperature dependent via the oxygen diffusion coefficient(Equation 2.4). In particular, an increase in temperature results in an increase in diffusion coefficient, and hence an increase in quenching response. The combined temperature dependence of the quenching process and the fluorescence intensity constitutes the overall temperature sensitivity of oxygen sensors.

Of the two fluorophores used here, the Ruthenium complex has the larger temperature sensitivity. This required careful temperature calibration and correction of the sensor. This is dealt with in Chapter 5.

## 2.8 Summary

This chapter has introduced the phenomena of fluorescence and fluorescence quenching. The oxygen-sensitive fluorophores used throughout this project have been described and the technique used to make measurements on the films doped with these fluorophores has been introduced. The results of these measurements along with the conclusions that can be drawn from them are presented in Chapters 5 and 6.

# Bibliography


[1] C. Malins, H.G. Glever, T.E. Keyes, J.G. Vos, W.J. Dressick, and B.D. MacCraith. Sol-gel immobilised ruthenium(II) polypyridyl complexes as chemical transducer for ph sensing. *Sens and Act B*, 67:89–95, 2000.

[2] C. McDonagh, C. Kolle, A.K. McEvoy, D.L. Dowling, A.A. Cafolla, S.J. Cullen, , and B.D. MacCraith. Phase fluorometric oxygen sensor. *Sens and Act B*, 74:123–129, 2001.

[3] C. Malins, T.M. Butler, and B.D. MacCraith. Influence of the surface polarity of dye-doped sol-gel glass films on optical ammonia sensor response. *Thin Solid Films*, 368:105–110, 2000.

[4] Q. Chang, Z. Murtaza, J.R. Lakowicz, and G. Rao. A fluorescene lifetime-based solid sensor for water. *Analytica Chimica Acta*, 350:97–104, 1997.

[5] B. G. McLachlan and J. H. Bell. Pressure-sensitive paint in aerodynamic testing. *Experimental Thermal and Fluid Science*, 10:470–485, 1995.

[6] J. R. Lakowicz. *Topics in Fluorescence Spectroscopy, Vol. 2 - Principles.* Plenum Press, 1991.

[7] E. L. Wehry. *Modern Fluorescence Spectrometry 3.* Plenum Press, 1981.

[8] C. Kolle. Development of an optical dissolved oxygen sensor. *Dublin City University School of Physical Sciences, Unpublished*, 1999.

[9] G. O'Keeffe, B.D. MacCraith, A.K. McEvoy, C.M. McDonagh, and J.F. McGilp. Development of a LED-based phase-fluorimetric oxygen sensor using evanescent wave excitation of a sol-gel immobilized dye. *Sens and Act B*, 29:226–230, 1995.

[10] M. Choi and D. Xiao. Linear calibration function of luminescence quenching-based optical sensor for trace oxygen analysis. *Analyst*, 124:695–698, 1999.

[11] C.M. McDonagh, B.D. MacCraith, and A.K. McEvoy. Tailoring of sol-gel films for optical sensing of oxygen in gas and aqueous phase. *Analytical Chemistry*, 70:45–50, 1998.

[12] A.K. McEvoy. *Development of an Optical Sol-Gel-Based Dissolved Oxygen Sensor*. PhD thesis, School of Physical Sciences, Dublin City University, 1995. Unpublished.

[13] D.B. Papkovsky, G.V. Ponomarev, W. Trettnak, and P. O'Leary. Phosphorescent complexes of porphyrin keytones: Optical properties and application to oxygen sensing. *Analytical Chemistry*, 67:4112–4117, 1995.

[14] D.B. Papkovsky. Luminescent porphyrins as probes for optical (bio)sensors. *Sens and Act B*, 11:293–300, 1993.

[15] D. B. Papkovsky. New oxygen sensors and their application to biosensing. *Sens and Act B*, 124:695–698, 1999.

[16] D. B. Papkovsky, A.N. Ovchinnikov, V.I. Ogurtsov, G.V. Ponomarev, and T. Korpela. Biosensors on the basis of luminescent oxygen sensor: the use of microporous light-scattering support materials. *Sens and Act B*, 51:137–145, 1998.

[17] C. McDonagh, A.M. Shields, A.K. McEvoy, B.D. MacCraith, and J.F. Gouin. Optical sol-gel based dissolved oxygen sensor: Progress towards a commercial instrument. *Journal of Sol-Gel Sci. and Tech.*, 13:207–211, 1998.

# Chapter 3

# Fabrication of Sol-Gel Sensor Films

## 3.1 Introduction

Although most research into sol-gel materials occurred in the second half of the $20^{th}$ century, the sol-gel process has its origins back in the $19^{th}$ century. In 1846 a chemist named Ebelmen succeeded in preparing a metal alkoxide from $SiCl_4$ [1]. However this achievement went relatively unnoticed, with the exception of some chemists at the time, for a long time until researchers began to examine Ebelmen's work more closely [2]. Since that time great interest has built up around this process and much research has been carried out on sol-gel materials.

## 3.2 The Sol-Gel Process

The sol-gel process is a method for producing glassy materials as either thin films or monoliths at a much lower temperature than the normal glass production temperatures. Optical sensors can be produced using sol-gel thin films, as these glass films are porous and can have indicator dyes entrapped in their pores during their fabrication.

### 3.2.1 The Basic Process

The basic process involves the hydrolysis and condensation of an alkoxide precursor in the presence of water, a catalyst and solvent respectively [3]. This is shown in

the schematic diagram in Figure 3.1, and described by Equations 3.1, 3.2, and 3.3.

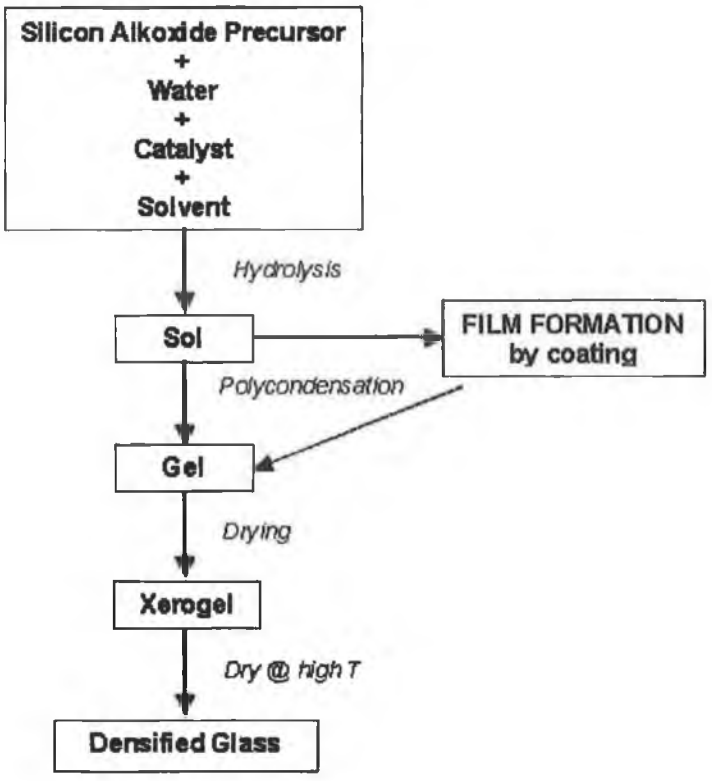


**Figure 3.1:** Outline of sol-gel process for fabrication of glass.

$$\equiv Si - OR \mid H_2O \quad \Leftrightarrow \quad \equiv Si - OH \mid ROH \tag{3.1}$$

$$\equiv Si - OR \mid HO - Si \equiv \quad \Leftrightarrow \quad \equiv Si - O - Si \equiv \mid ROH \tag{3.2}$$

$$\equiv Si - OH \mid HO - Si \equiv \quad \Leftrightarrow \quad \equiv Si - O - Si \equiv \mid H_2O \tag{3.3}$$

To fabricate glass using the sol-gel process water(of a pre-defined pH value) is added to the alkoxide precursor. For these two normally immiscible fluids to mix a mutual solvent is used. During this work an alcohol was used as the solvent. These three components of the sol are all added while the sol is constantly mixed. This is performed using magnetic stirring. Entrapment of the indicator dyes used in optical oxygen sensors normally occurs at this "adding and stirring" stage. Hydrolysis and condensation reactions begin and continue while the sol is left mixing as it is aged for a time. This is carried out until it becomes viscous enough to coat onto a substrate.

The gels formed from the above reactions undergo a temperature program which is designed to complete the reactions and dry the films or monoliths, making them into a hard glass material. If the drying temperature is kept below 200°C the glass is non-densified and porous. For this application a porous structure enables molecular oxygen to diffuse into the sol-gel film and quench the fluorescence of the entrapped fluorophore.

It is this controlling of the drying temperature, along with control of the other parameters involved in the sol-gel process(e.g. the water to precursor ratio (R) value, pH, type of precursor) that allows the properties of the sensor films to be tailored to suit the needs of the particular application[4].

### 3.2.2 Influence of Process Parameters on Film Properties

Along with their optical purity and robustness, the ability to control the process parameters and influence the sensor film properties is a major advantage that the sol-gel process has over polymer films. There are many process parameters that can be varied in an attempt to control the sol-gel film properties.

The major parameters used to tailor the films are the water to precursor ratio(R), the pH of the sol, the ageing time and temperature, and the catalyst used.

The **type of silicon precursor used** in the sol formulation is a major parameter that affects the properties of the fabricated films. The type of precursor used can affect the way in which the resultant thin film reacts to water. Tetraethoxysilane(TEOS)-based sol-gel films are largely hydrophilic, as the surface groups attract water molecules. These water molecules on the surface of a film can reduce the response of the film to the presence of molecular oxygen and increase the response time of the sensor. They can also assist in the leaching of the fluorescent dye out of the sensor film[4], which is not advantageous when the sensor is to be used in a water tank. An organically modified precursor(ORMOSIL) such as Methyltriethoxysilane(MTEOS)

that produces largely hydrophobic sol-gel films is therefore a better choice for this application[5]. These films repel the water molecules from their surface which promotes the diffusion of oxygen into the sensor matrix. This in turn improves the sensor performance.

The **water to precursor ratio** or **R** value, affects the rate at which the hydrolysis and condensation reactions occur. This in turn has an effect on the viscosity of the sol and finally on the sensor films. In general an increase in the R value, that is an increase in the amount of water present in the sol, results in an increase in the rate of hydrolysis and condensation. This has the effect of making the sol more viscous and the resulting sol-gel sensor films more dense. In the context of this work(and previous research carried out at DCU into $[Ru(Ph_2phen)_3]^{2+}$-based optical oxygen sensors) it was observed that sensor films made from a sol with a R-value of 2 had a larger pore size than those made from a $R = 4$ sol[4]. This is in keeping with the fact that the films produced from a higher R-value sol have a higher density.

The **pH value** of a sol can also greatly affect the final properties of the sensor films. The pH of the sol is quite easily controlled by controlling the amount of acid introduced into the water, before it is added to the sol. For silica-based materials, the isoelectric point occurs at a pH value of approximately 2[4, 6]. The isoelectric point is the point along the pH scale where the electron mobility and the surface charge is zero, that is to say when the net charge on the particular molecule is zero. This pH value provides the boundary between acid and base catalysis. In general, an acid-catalysed sol is defined as one with a pH value below 2, and a base-catalysed sol is one with a value higher than 2. Low pH conditions, or acid catalysis promotes a fast rate of hydrolysis and a slower rate of condensation. These conditions lead to a fine network structure of cross linked linear chains which causes the pore size of the sensor films to be smaller. In base-catalysed sols, the rate of hydrolysis is reduced and that of the condensation reactions is increased. These conditions promote larger colloidal particles with greater pore sizes between them.

A more rigorous and detailed discussion on the effect the pH value has on a sensor film's properties is given by Klein [2, 6]. It is clear that the pH value of a sol has a profound effect on its porosity.

The **ageing time** can also affect the film properties of sol-gels. The ageing time is the time that the sol is allowed to stand before being coated onto a substrate. The temperature at which the sol is allowed to stand is also a factor. During this

process the hydrolysis and condensation reactions continue. The rate at which they do is determined by whether the sol is left to stand at room temperature or at a higher temperature, and whether or not it is agitated or stirred. During this work both room temperature and higher temperature ageing methods were used, in an effort to determine the optimum ageing conditions for the sensor film required.

## 3.3 Fabrication of Ruthenium-Doped Sol-Gel Films

As stated in Section 2.3 the fluorophore used for the majority of the work reported here is $[Ru(Ph_2phen)_3]^{2+}$. It is this complex, entrapped in an MTEOS-based sol-gel film, that has been used in the optical oxygen sensor for waste-water monitoring reported here. The formulation used to make these sensor films was developed by researchers at the Optical Sensors Laboratory(OSL) at DCU. An R-value of 4 was used to minimise dye leaching. This has previously been reported[4].

A clean glass vial containing a magnetic bob was placed on a balance to allow the various quantities of the constituents of the sol to be measured accurately. This magnetic bob, in conjunction with the magnetic stirrer would be used to mix the precursor, water and solvent during the process. The $[Ru(Ph_2phen)_3]^{2+}$ complex was added to the vial, followed by the absolute alcohol. This solution of $[Ru(Ph_2phen)_3]^{2+}$ and Ethanol was stirred magnetically until all the Ruthenium was dissolved in the solvent. Water whose pH value had been changed to 1 by the addition of Hydrochloric acid (HCl), was added next, and again the solution was magnetically stirred. While the solution was stirring, the MTEOS was added in a dropwise fashion from a pipette. The entire sol was then stirred for 1 hour, with the lid of the vial replaced loosely.

The, by now, more viscous sol was ready to be coated onto the chosen substrate. These substrates are discussed in Section 3.5 and the techniques used to coat them in Section 3.6.

## 3.4 Fabrication of Porphyrin-Doped Films

During the course of this work the porphyrin, PtOEPk, was incorporated into several different support matrices. These support matrices included various sol-gel films of varying type, soluble ormosil films and polymer films. These are all discussed below.

### 3.4.1 Porphyrin-Doped Sol-Gel Films

Several sol-gel formulations were investigated as support matrices for PtOEPk during the porphyrin section of this work. This was done so as to find the optimum sol-gel method for use with the chosen porphyrin. Historically porphyrins have been difficult to incorporate into sol-gel films. Some work has been published[7, 8] but no long term stability data has been reported. In this work a number of formulations were successful in incorporating these dyes into sol-gel thin films, and the long term stability of these films looks promising. Sol-gel parameters that were varied during this optimisation process included:

- the type of precursor used (TEOS, MTEOS, TESPIC[(Triethoxysilyl)propyl isocyanate])
- the pH of the sol
- the R value of the sol
- the ageing time allowed and the temperature of the sol during this period

A non-hydrolytic sol-gel formulation was also tried during the course of this work. This is a sol that includes no water[9], but instead is made using a silicon-based precursor, as before, along with silicon tetra chloride($SiCl_4$). It is thought that water may have been chemically denaturing the porphyrin, resulting in the reduction of the phosphorescence.

Four non-hydrolytic formulations were tried in total. They involved mixing the silicon-based TEOS precursor with a quantity of $SiCl_4$ and also with a combination of $SiCl_4$ and iron chloride($FeCl_3$). The amount of $SiCl_4$ was varied and also the mixture of $SiCl_4$ and $FeCl_3$ was changed to investigate the effect on the film quality. The films produced using this non-hydrolytic method were of very poor quality and not suitable for optical oxygen sensing. This method was not further pursued.

The successful sol-gel formulations for PtOEPk doped films are detailed below.

1. **TEOS-based PtOEPk Sol-Gels.** Tetraethoxysilane(TEOS) was used as a precursor in the first PtOEPk doped sol-gels. A range of values of pH were used with TEOS as the precursor. A highly acid-catalysed sol was made using a pH of 1 and a highly base-catalysed sol was made using a pH of 11. Intermediate pH values of 4, 7, and 9 were also tried. All the films provided a response to changing oxygen concentrations, but some were noticeably

better than others. The best was pH4. The manner in which these sensor films were tested is discussed later in Chapter 5, as are the results obtained.

2. **MTEOS-based PtOEPk Sol-Gels.** Methyltriethoxysilane(MTEOS) was the second precursor that was investigated while doping sol-gels with PtOEPk. Again a number of pH values were used in an effort to get an optimum sol-gel for PtOEPk entrapment. An acid pH of 1 was tried along with a base-catalysed pH of 4. These two pH values were identified due to the fact that they had produced the best films during the TEOS-based sol-gel testing. The MTEOS-based sensor films showed a marked improvement from the TEOS-based films. Results are presented in Chapter 6.

3. **TESPIC-based PtOEPk Sol-Gels.** TESPIC is another silica precursor that was investigated for its potential to entrap PtOEPk in a sol-gel matrix. This precursor was tried due to its more polar nature than both TEOS and MTEOS. It was thought that this increased polarity might assist the entrapment of the porphyrin in the sol-gel host matrix. The results for this particular precursor were encouraging and also similar to those of the MTEOS-based sol-gels. They are again presented in Chapter 6.

### 3.4.2 Porphyrin-Doped Soluble Ormosil Films

A second support matrix that was investigated for the entrapment of the PtOEPk porphyrin was a hybrid matrix known as a soluble ormosil. Soluble ormosils combine the features of both polymer and sol-gel based films. They are soluble in organic solvents like polymers, and are mechanically stable like sol-gels. Their main advantage with respect to this work is their sol-gel like porous structure, that allows them to be doped with indicator dyes, such as PtOEPk. The soluble ormosil formulation used here creates rigid glass support matrix for the PtOEPk porphyrin. The ormosil glass adheres well to the substrates chosen for use in this work, as discussed in Section 3.5.

The ormosil glass was synthesized according to a formulation that was developed at the University of Regensburg in Germany by Klimant et al.[10]. Using this ormosil glass the sensor films, doped with PtOEPk were produced as detailed below.

The production of this PtOEPk-doped soluble ormosil cocktail was similar to the production of the $[Ru(Ph_2phen)_3]^{2+}$-doped sol. A clean glass vial containing a magnetic bob was used. Several milligrams of the synthesized ormosil glass, along

with the PtOEPk dye was dissolved in chloroform. This cocktail was stirred magnetically to dissolve the constituents. This cocktail was allowed to age for 1 hour until it was viscous enough to be coated onto the chosen substrate. The films coated on these substrates were placed in an oven at 70°C for 18 hours to dry.

The sensor films made using the above procedure produced fast response to changes in oxygen, less than 10s response time from 0% – 100% oxygen, and both the intensity and phase-shift signals were comparable to those of polymer films.

### 3.4.3 Porphyrin-Doped Polymer Films

The final support matrix investigated for use with PtOEPk was an ethyl cellulose polymer. It has been widely reported that PtOEPk has successfully been entrapped in various polymer films. Indeed the aim of this work was to successfully incorporate this porphyrin into a sol-gel film due to the advantages these sensor films have over polymer films. Polymer films were fabricated in the laboratory for comparison purposes. The porphyrin doped films using the white Millipore filter paper as a substrate(see Section 3.5), were also used with the commercial fibre-based system described in Section 6.3. The results obtained were excellent and in good agreement with the results obtained by others using similar sensor films[11]. These results along with the results of all the other support matrices are presented and analysed in Chapter 6.

## 3.5 Substrates Used

Several different types of substrate were experimented with and used during the course of this work with both $[Ru(Ph_2phen)_3]^{2+}$ and PtOEPk fluorescent complexes. Concerning the $[Ru(Ph_2phen)_3]^{2+}$-doped films used with the DO waste-water monitoring probe, work had previously been done optimising the substrate used. A dedicated perspex disc, shown in Figure 3.2, was designed by researchers in the OSL at DCU, to fit inside the probe head, which will be described further in Chapter 4. The dimensions and shape of this disc are shown in Figure 3.2[12].

This disc was manufactured from perspex(Polymethyl Methacccrelate - PMMA) due to its excellent optical properties, the ease with which it can be machined and its resistance to corrosion(a major problem in the waste water industry, as discussed in Section 5.6).

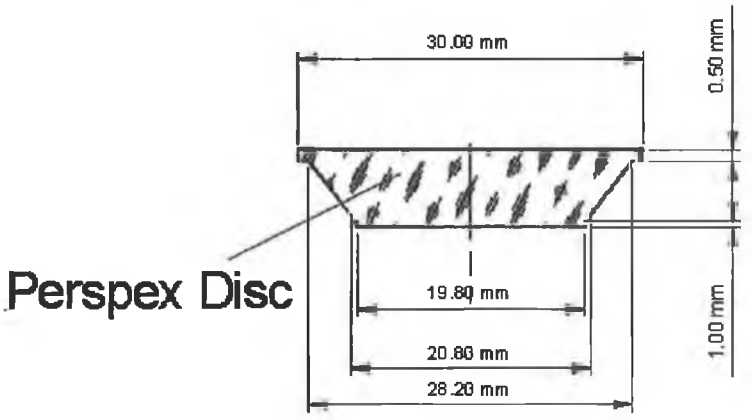


**Figure 3.2:** Shape and Dimensions of Perspex Disc used in DO Waste Water Probe.

During the PtOEPk work portion of this project different substrates were investigated and tested for ease of use and quality of fluorescence signal produced. They included glass slides, perspex, overhead acetates, polyethylene film and a white Durapore® filter paper manufactured by Millipore, UK. This white Durapore® filter paper, which has a pore size of 0.22$\mu$m, was adopted as a support matrix by Papkovsky et al.[11], and it was also used here as it was compatible with the fibre-based characterisation system discussed in Chapter 6. It has the effect of scattering the excitation light, thus illuminating more of the sensor film and producing more fluorescence.

Some of the substrates proved very useful for this work, while others despite their popularity as a substrate for optical sensors, did not lend themselves well for use with the fibre-based sensor system described in Section 6.3.1. One such substrate which did not suit well was glass. These soda-lime glass slides(or ordinary microscope slides) have been used extensively within the OSL as a substrate in characterisation of fluorescence quenching sensor films[13]. However the shape of the sensor film required for work with the PtOEPk complex, coupled with the shape of the flow cell used in the experiments(both circular) was not easily produced using glass slides.

The main substrates used, which were compatible with the fibre-based system described in Chapter 6, were circular discs made from overhead acetates and polyethylene film. Both of these substrates are optically transparent and could be cut easily into the 10mm discs required. This could be done either before or after the substrates had been coated with the sensor films. Both of these substrates were very

thin, approximately 0.5mm each. As mentioned previously the final substrate that was used during this work was a white Durapore® filter paper manufactured by Millipore(UK). The use of this substrate in optical oxygen sensing and its unique properties have been described in detail by Papkovsky et al.[11]. The pore size of this filter paper is $0.22\mu$m.

### 3.5.1 Cleaning of Substrates

It is important to ensure that before a sol-gel is coated onto any substrate that the surface of the substrate is clean and free of dirt. Most of the substrates used in both the work with $[Ru(Ph_2phen)_3]^{2+}$ doped films and PtOEPk doped films were cleaned in a similar fashion. The only substrates that were not cleaned were the durapore filter paper substrates. For these a clean area of the roll of filter paper purchased from Millipore was cut out and used.

The perspex, overhead acetates and polyethylene film substrates were all cleaned by firstly washing them with de-ionised water. They were then wiped with methanol and then washed again with de-ionised water. The substrates were finally allowed to dry in air before being coated. Glass slides used in this work were cleaned using the same process except for an additional wiping with acetone after being wiped with methanol, and before being washed a second time with de-ionised water. Acetone could not be used on perspex, overhead acetates or polyethylene film as it is too harsh a solvent and damaged these substrates.

## 3.6 Coating Techniques

There are several coating techniques available for depositing sol-gels onto a chosen substrate. They include spin-coating, dip-coating, stamp-printing, screen-printing, or simply dropping the sol onto the substrate using a pipette. The first two methods provide thin films that are extremely uniform, and which can be reproduced readily[14]. They are however not suited to all applications. For most of this work the films were pipetted onto the substrates. The uniformity of these films is of a high enough quality for this work. The spots generated were of an ideal size and shape for use with the two sensor configurations detailed in Chapter 4.

A $\mu$-pipette was used to pipette small amounts of the dye doped sol onto the substrate. A typical volume of $4\mu$l of sol was used as this produced a spot of ideal size for this work. The drop of sol from the $\mu$-pipette was allowed to drop freely

onto the clean substrate in a draught and vibration free environment. The coated substrates were allowed to stand for a short while before being transferred to an oven for drying. This was done so that the sol would begin to gel and would not spread during movement to the oven. This process is shown in Figure 3.3.

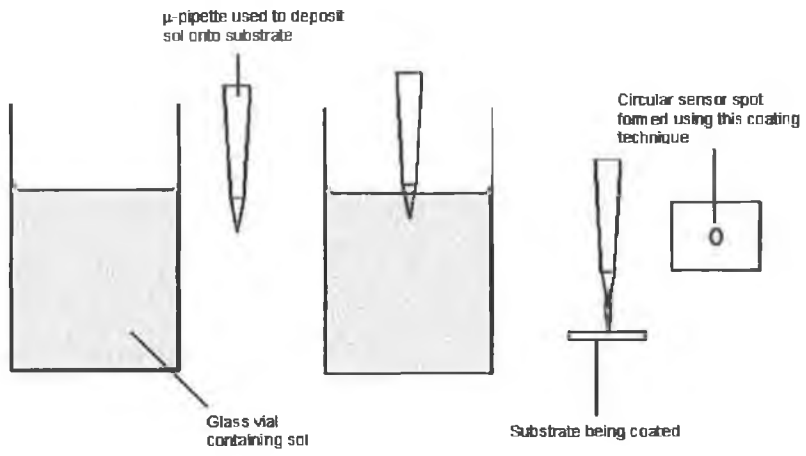


**Figure 3.3:** $\mu$-pipetting technique used to coat substrates.

The spin-coating technique was also used during the course of this work. It was not used to coat a sol onto a substrate however, but rather to coat an optical isolation layer(OIL) on top of an $[Ru(Ph_2phen)_3]^{2+}$ coated perspex disc(the type shown in Figure 3.1) for use with the DO waste water monitoring probe. This was done to remove the interference effects that any outside light may have had on the performance of the DO waste water monitoring probe. Black silicone rubber(Wacker Elastosil N189) was used for this optical isolation layer. A small amount of this black rubber dissolved in toluene was placed in the middle of the disc. The disc was secured into the spin-coater using the vacuum chuck provided and rotated at high speed. The rubber coating formed over the sol-gel sensor spot, preventing any light from passing through the disc. The thickness of this layer of black rubber was chosen so as not to affect the response time of the sensor. This rubber coating also serves to prevent fouling of the sensor spot by its aqueous environment.

## 3.7 Summary

This chapter has introduced the sol-gel process which was used to produce the majority of sensor films used throughout this work. The various optimised sol-gel

formulations, and the factors used during their optimisation are detailed. Also introduced here are the other methods by which the support matrices for the indicator dyes were made, the soluble ormosil method and the polymer method. The details of these methods and the properties of the sensor films they produced are discussed. The selection of substrates for this project and the techniques used to coat them are described, and the reasons for their selection are given.

# Bibliography


[1] J. J. Ebelmen. The sol-gel process. *Chemical Review*, 90:33–72, 1990.

[2] C. J. Brinker and G. W. Scherer. *Sol-Gel Science: The Physics and Chemistry of Sol-Gel Processing.* Academic Press, 1990.

[3] L. L. Hench and J. K. West. The sol-gel process. *Chemical Review*, 90:33–72, 1990.

[4] C.M. McDonagh, B.D. MacCraith, and A.K. McEvoy. Tailoring of sol-gel films for optical sensing of oxygen in gas and aqueous phase. *Analytical Chemistry*, 70:45–50, 1998.

[5] C. McDonagh, A.M. Shields, A.K. McEvoy, B.D. MacCraith, and J.F. Gouin. Optical sol-gel based dissolved oxygen sensor: Progress towards a commercial instrument. *Journal of Sol-Gel Sci. and Tech.*, 13:207–211, 1998.

[6] L. C. Klein. *Sol-Gel Technology for Thin Films, Fibres, Preforms, Electronics, and Speciality Shapes.* Noyes Publications, 1988.

[7] S. K. Lee and I. Okura. Optical sensor for oxygen using a porphyrin-doped sol-gel glass. *The Analyst*, 122:81–84, 1997.

[8] S. K. Lee and I. Okura. Porphyrin-doped sol-gel glass as a probe for oxygen sensing. *Analytica Chimica Acta*, 342:181–188, 1997.

[9] J. Hay, D. Porter, and H. Raval. A non-hydrolytic route to organically-modified silica. *Chem. Comm.*, pages 81–82, 1999.

[10] I. Klimant, F. Ruckruh, G. Liebsch, A. Stangelmayer, and O. S. Wolfbeis. Fast response oxygen micro-optodes based on novel soluble ormosil glasses. *Mikrochimica Acta*, 131:35–46, 1999.

[11] D. B. Papkovsky, A.N. Ovchinnikov, V.I. Ogurtsov, G.V. Ponomarev, and T. Korpela. Biosensors on the basis of luminescent oxygen sensor: the use of microporous light-scattering support materials. *Sens and Act B*, 51:137–145, 1998.

[12] C. McDonagh, C. Kolle, A.K. McEvoy, D.L. Dowling, A.A. Cafolla, S.J. Cullen, , and B.D. MacCraith. Phase fluorometric oxygen sensor. *Sens and Act B*, 74:123–129, 2001.

[13] A. K. McEvoy, C.M. McDonagh, and B.D. MacCraith. Dissolved oxygen sensor based on fluorescence quenching of oxygen-sensitive ruthenium complexes immobilised in sol-gel derived porous silica coatings. *Analyst*, 121:785–788, 1996.

[14] I. Strawbridge and P. F. James. Thin silica films prepared by dip coating. *Journal of Non-Crystalline Solids*, 82:366–372, 1986.

# Chapter 4

# Oxygen Sensor Configurations

## 4.1 Introduction

Oxygen sensors can be used in a wide variety of applications, from respiratory monitors in breathing apparatus[1], to instruments for making in-vivo analysis of blood[2], to the waste water application associated with this project. Oxygen sensors can also have several different principles of operation, of which electro-chemical methods and optical fluorescence quenching are two. An example of an electro-chemical oxygen sensor is the Clark electrode probe, this type of probe was first developed by L.C. Clark in 1956 [3]. This type of specific oxygen sensor is available in many different configurations. An example of one configuration is the YSI hand-held (Model 55, YSI Inc., Ohio, USA) probe which has been used in the OSL at DCU for comparison measurements with sensors developed in house. The operation of this YSI hand-held probe is electro-chemically based. A diagram of this hand-held portable oxygen probe is shown in Figure 4.1.

The optical configuration for fluorescence quenching based sensors developed in the laboratory has evolved over a number of years. Both fibre-based and planar waveguide configurations have been used[4, 5]. The details of the configuration developed for the DO waste-water sensor are described here. Also discussed is the set-up and configuration associated with the fibre-based sensor which was used to make measurements with the porphyrin-based sensor films.

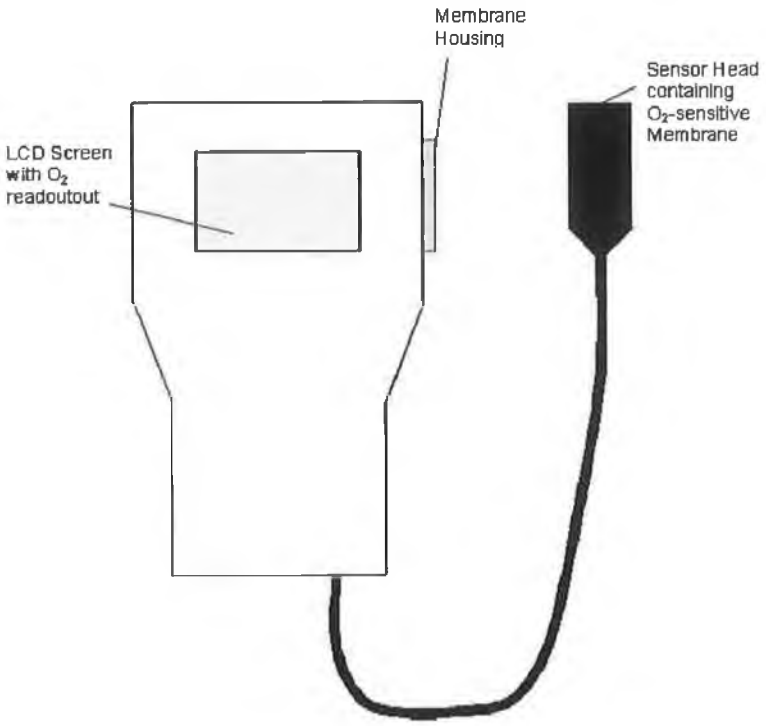


**Figure 4.1:** YSI hand held Clark electrode type probe.

## 4.2 DO Waste Water Monitoring Probe Configuration

As already stated above the DO waste-water monitoring probe that was tested and characterised during the course of this project evolved over several years research at DCU to its current status. One of its earliest and most basic forms is shown in Figure 4.2(Early light-sample-detector). This diagram shows a fluorescent sample being illuminated by an excitation source which is optically filtered so as to only allow through light that will excite the sample. Similarly on the detector side of the sample the light is again optically filtered so as to only allow through the fluorescence of the sample.

From this, the sensor evolved to use LED excitation and photodiode detection in a system that could reference out any background light. Flow cells for both gas and water were designed so that laboratory tests could be carried out in gaseous and aqueous states respectively. These oxygen measurements were initially carried out using an intensity-based method but when this proved unreliable, as described in Chapter 2, a lifetime measurement method was adopted. The evolution of oxygen

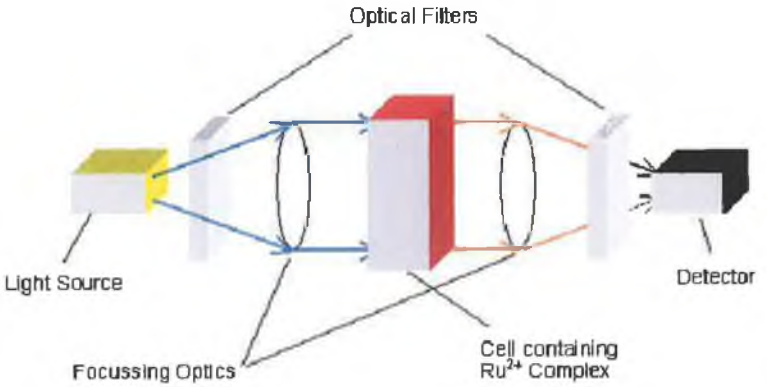


**Figure 4.2:** Early light-sample-detector set-up.

sensors has already been described[6, 7, 8]. The current phase fluorometric prototype probe sensor is shown schematically in Figure 4.3.

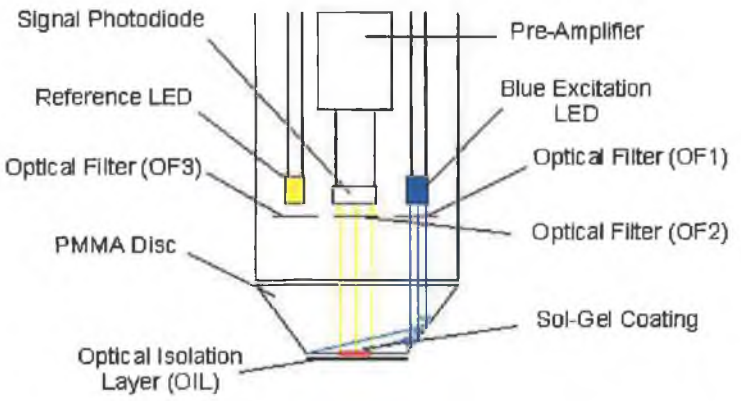


**Figure 4.3:** Schematic of Probe Head of DO Waste Water System.

This probe configuration consists of a replaceable cap that contains the $[Ru(Ph_2phen)_3]^{2+}$-doped sensing spot, with the OIL coated on top, and a main body, which measures approximately 15cm in length and 4cm in width, which contains the optoelectronics components(LEDs, PD) as well as the initial amplification electronics. These electronics were designed in-house by a previous researcher. They are described further in Chapter 5 and detailed circuit diagrams are given in Appendix I. The schematic diagram above in Figure 4.3 also shows how the sensor spot is illuminated by the blue excitation LED and how the fluorescence and reference

light are detected by the PD. The function of the reference LED shown in Figure 4.3 is described in detail in Section 5.2.1. This illumination of the centred sensor spot by the off-centred excitation LED is a major design feature of the probe configuration.

As shown in Figure 3.2 and discussed in Section 3.5, the perspex disc used as the substrate for the sol-gel sensor spot has been carefully designed. This has been done so that the light from the off-centred blue LED is totally internally reflected within the perspex disc onto the centred sensor spot. This total internal reflection(TIR) is achieved by virtue of an air gap that exists between the perspex disc and the cap. Great care must be taken when attaching the perspex disc to the cap of the probe not to eliminate this air gap, and thus eliminate the TIR of the blue excitation light. Without this feature the current probe configuration would not allow the sensor spot to be properly excited by the blue LED and the fluorescence from this spot would be greatly reduced. This TIR process is shown more clearly in Figure 4.4

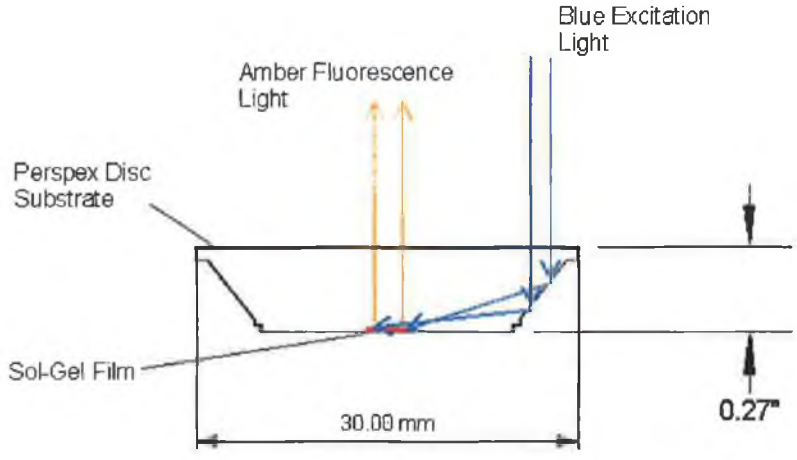


**Figure 4.4:** Total Internal Reflection (TIR) Occurring in Probe Cap.

Of vital importance to the quality of the output signal from this oxygen probe is the proximity of the PD to the first stage amplification electronics(contained in the probe head). The PD has to be close to the amplification electronics to minimise the noise pickup which would degrade the output signal. The output signal from this first stage of amplification electronics is passed to a separate control box via a cable. Here further signal amplification and signal processing occurs. The phase shift $\phi$ corresponding to the oxygen concentration being investigated is measured here. A voltage corresponding to the $\phi$ detected is passed to an A/D card(National Instruments, PC516) and analyzed by the software. This software was written in

house for use with this sensor system using LabVIEW[9].

Also contained in the probe head is a thermistor(Betatherm NTC 30K6A1). This is used to record the temperature at a point in the probe head very close to the sensor film. This is taken as a good estimation of the sensor film temperature. The signal from this thermistor is also sent, via the control unit where it is amplified, to the A/D card in the data processing computer. It is recorded along with the $\phi$ data and is used to compensate for any changes in the temperature. This compensation is performed using dedicated software designed for this sensor system. The fluorescent complexes dependence on temperature was described in Section 2.7 and the temperature compensation procedure is detailed in the calibration protocol in Section 5.4.2. A final piece of data that is recorded by this sensor is the ambient air pressure. This pressure sensor(Sensor Technics HCX001A6V) is not contained in the probe head but in the control box of the system, and measures ambient air pressure. This pressure data, like the temperature data recorded from the thermistor, is used to compensate for any changes in ambient air pressure. This routine is detailed in Section 5.4.2. A diagram of the entire system associated with the DO monitoring probe is shown in Figure 4.5 below.

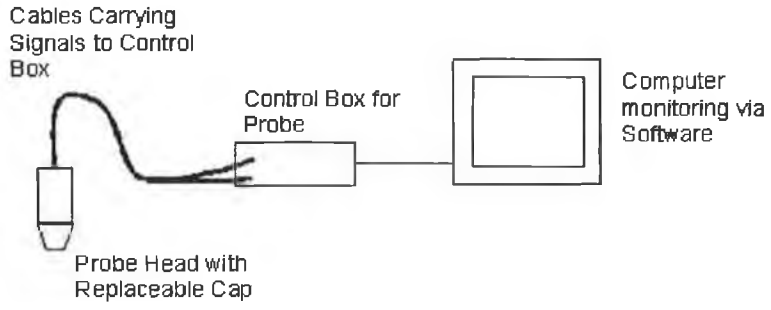


**Figure 4.5:** Entire System Associated with DO Waste Water Probe.

A major feature of this probe configuration is that it is totally sealed and watertight. It is also very rugged and compact so that it can be field tested in the harsh working environment of a waste-water treatment plant. An initial phase of field testing has already taken place.

The detection method and measuring instrumentation is discussed further in Section 5.2.2, along with the results of the laboratory and field testing of the DO monitoring probe. The calibration protocol associated with this sensor is also described.

## 4.3 Fibre-Based Porphyrin Sensor Configuration

A fibre-based sensor system was also used during the course of this work. This sensor system was designed externally[10] specifically for work with the PtOEPk porphyrin. The system was purchased for the testing and characterisation of the PtOEPk doped oxygen sensitive films described in Section 3.4, the results of which are presented in Chapter 6. These measurements were made using the phase fluorometric method detailed in Section 2.6. A detailed description of the fibre-based system is given Section 6.3.

## 4.4 Summary

The configurations of the two sensor systems used throughout this project have been detailed in this chapter. The $[Ru(Ph_2phen)_3]^{2+}$-based dissolved oxygen set-up has been shown diagrammatically and described in great detail. The results achieved from oxygen experiments conducted with these sensor configurations are presented in the following two chapters; Chapters 5(DO waste-water monitoring probe) and 6(Fibre-based porphyrin sensor system). Where possible, comparisons are drawn between the two systems and their performances.

# Bibliography


[1] T. O'Riordan, D. Buckley, V. Ogurtsov, R. O'Connor, and D.B. Papkovsky. A cell viability assay based on monitoring respiration by optical oxygen sensing. *Analytical Biochemistry*, 278:221–227, 2000.

[2] A.J. Schwalb, K.A. Richman, and D.R. Jobes. Continuous in-vivo blood-gas determination in man: Reliability and safety of a new device. *Anesthesiology*, 52:313–317, 1980.

[3] L.C. Clark. Monitor and control of blood and tissue tensions. *Trans. Amer. Artif. Intern. Organs*, 2:41, 1956.

[4] B.D. MacCraith, C.M. McDonagh, G. O'Keeffe, E.T. Keyes, J.G. Vos, B. O'Kelly, and J.F. McGlip. Fibre-optic oxygen sensor based on fluorescence quenching of evanescent-wave excited ruthenium complexes in sol-gel-derived porous coatings. *Analyst*, 118:385–388, 1993.

[5] J.F. Gouin, A. Doyle, and B.D. MacCraith. Fluorescence capture by planar waveguide as platform for optical sensors. *Electronics Letters*, 34:17, 1998.

[6] A.K. McEvoy. *Development of an Optical Sol-Gel-Based Dissolved Oxygen Sensor.* PhD thesis, School of Physical Sciences, Dublin City University, 1995. Unpublished.

[7] A. Shields. Development of an optical dissolved oxygen sensor. Master's thesis, School of Physical Sciences, Dublin City University, 1999. Unpublished.

[8] C. McDonagh, A.M. Shields, A.K. McEvoy, B.D. MacCraith, and J.F. Gouin. Optical sol-gel-based dissolved oxygen sensor: Progress towards a commercial instrument. *Journal of Sol-Gel Sci. and Tech.*, 13:207–211, 1998.

[9] National Instruments. *User Manual.* National Instruments, 1998.

[10] D.B. Papkovsky, G.V. Ponomarev, W. Trettnak, and P. O'Leary. Phosphorescent complexes of porphyrin ketones: Optical properties and application to oxygen sensing. *Analytical Chemistry*, 67:4112–4117, 1995.

# Chapter 5

# Calibration and Testing of the Prototype Dissolved Oxygen Sensor

## 5.1 Introduction

In this chapter the characterisation, testing and calibration of the prototype DO waste-water monitoring probe is presented. The specifications set down in conjunction with the industrial partner associated with this section of work are outlined. Results from the extensive laboratory testing carried out, as well as results from the initial phase of field testing are presented. The response of the sensor to changing concentrations of oxygen is shown and characterised, and the performance parameters that affect this response are discussed.

The calibration protocol associated with this sensor is described in detail, with each individual step explained and justified. Results from the first phase of field testing along with the modifications made to the prototype probe after the field testing are described. The re-characterisation of this newer prototype sensor is outlined, along with the difficulties encountered after these modifications were made. The current status of the system is assessed.

## 5.2 Probe Design and Electronic Measuring Instrumentation

The design of this prototype probe and the factors that affected its design have been discussed in detail in Chapter 4. Schematic diagrams of both the probe head and the entire sensor system are shown in Figure 4.3 and Figure 4.5 respectively. The circuit diagrams of the electronic instrumentation, both from the probe head and the control unit of the sensor can be found in Appendix I. This section deals with the design and operation of this electronic measuring instrumentation, and how this impacted on the design of the probe itself.

### 5.2.1 Probe Design

As discussed in Chapter 4, the complete DO sensor consists of the probe head(shown in Figure 4.3) and the electronic control unit. The waste water application demanded that the probe head be small in size, as well as being rugged and with a disposable cap. The design considerations associated with the perspex sensor disc were discussed in Chapter 4. The blue LED (NSPB500, Nichia, Japan) shown in Figure 4.3 excites the sensor film via total internal reflection in the disc. The second, or reference LED (HLMP-DL08, Hewlett Packard), shown in the figure was introduced in order to correct for phase-shifts introduced in the electronics. It's temperature characteristics were matched very closely with the blue Nichia LED, which factored out the phase-shifts introduced by changing temperature. This LED has an emission spectrum in the range of the ruthenium complex fluorescence wavelength(600nm) and passes through the emission filter in front of the photodiode (S1223, Hamammatsu, UK). By switching alternately between the two LEDs, the phase-shift($\phi_{ref}$) of the detection circuitry can be exclusively determined. This reference phase is subtracted from the signal phase to give a phase angle $\phi$ which is related to $[O_2]$.

In this system the LEDs were carefully selected to ensure equal switching time characteristics and equal temperature behaviour. Figure 5.1 shows a schematic diagram of the complete system including optoelectronic and electronic components. The electronics are described in the next section.

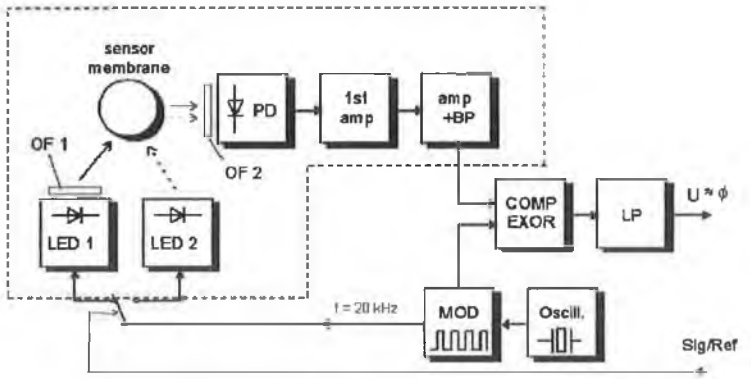


**Figure 5.1:** Schematic of Electronics Units of Entire Sensor System.

### 5.2.2 Electronic Instrumentation

This section deals with the operation of the electronic measuring instrumentation contained in both the probe head and the control unit. A schematic diagram of these components is shown in Figure 5.1. In this diagram those components inside the heavy bold dashed line are located inside the probe head, and those outside the dashed line are located in the control unit of the system. The main sections of these electronic measuring units are now explained individually.

**LED Driving Circuit:** This driving circuit is located in the control unit of the sensor system. It modulates the LEDs at the required frequency. The choice of modulation frequency is dependent on the indicator dye used in the sensor, and for the ruthenium dye used in this sensor it was chosen as 20kHz[1, 2, 3]. This value of 20kHz was chosen as a compromise between oxygen sensitivity and signal-to-noise ratio(SNR) in the phase system. While higher modulation frequencies result in greater $\phi$ values, and hence greater sensitivity, the demodulation factor, and hence the SNR decreases[4]. This modulation frequency of 20kHz is generated by a crystal oscillator(Epson SPGB8640BN), which is programmed using dip switches to the desired frequency. The remainder of the LED driving circuitry shown in Appendix I is matched as closely as possible to the band gap of the LED used. This is performed so as to optimise the operation of the LED.

**Photodiode and $1^{st}$ Amplifier Stage:** Both the PD and the first

amplifier stage of the processing electronics are located in the probe head, as explained previously. Here the light signals from the fluorescence of the sensor spot and the reference LED are detected by the PD. These signals are amplified for the first time by the amplification electronics located here.

**Further Amplification and Band-Pass Filtering:** This is the final part of the electronic instrumentation to be contained in the probe head. It consists of simple RC filter circuits, along with another op-amp based amplification circuit. The values of the resistive components used here(resistors and capacitors) have been carefully selected so as to optimize the performance of the $[Ru(Ph_2phen)_3]^{2+}$-based sensor at 20kHz.

**Comparator and Exclusive-OR Gate:** Upon entering the control unit of the system the signals from the probe head are amplified further and sent to a comparator chip(LT1016). This component produces a TTL-signal which, together with the excitation signal produced by the crystal oscillator, is fed to an exclusive-OR(EXOR) gate(CD74HCT86E). This produces a pulse width modulated(PWM) signal

**Low-Pass Filter:** This is the final portion of the electronic measuring instrumentation of this sensor system. The input signal to this low-pass filter is the PWM signal from the EXOR gate described above. The output signal produced by this filter is a d.c. voltage that corresponds to the phase-shift($\phi$) measured, and thus corresponds to the concentration of oxygen measured.

Data acquisition and analysis are achieved via a PC and A/D interface card. The phase shift, $(\phi_{sig} - \phi_{ref})$ is recorded together with the temperature and pressure and processed in the software to give temperature and pressure-corrected calibration curves.

## 5.3 Specifications of the Sensor

For this project detailed specifications were set down in conjunction with the industrial partner before the prototype probe was designed.

These target specifications detailed the level of performance that was expected of the prototype system in order for it to be tested in a waste-water treatment plant. The specifications and performance of this new sensor system had to be at least

as good as that of the conventional electrochemical Clark electrode type oxygen sensor. Preferably this new oxygen sensor system would perform better and have higher final specifications. The specifications that were agreed upon are listed in Table 5.1.

| **Specification** | **Specified** | **Achieved** |
|---|---|---|
| Measurement Range | 0 – 15ppm | 0 – 15ppm |
| Working Temperature Range | 0 – 40°C | 0 – 30°C |
| Resolution | 0.01ppm | 15ppb |
| Limit of Detection(LOD) | < 10ppb | < 6.6ppb |
| Stability of Measuring Electronics with Temperature | ✓ | ✓ |
| Ability to Compensate for Temperature and Pressure Changes | ✓ | ✓ |
| Single Point Calibration | ✓ | ✓ |

Table 5.1: Specifications of DO Sensor System

As is shown in the following section all of these specifications have been achieved, and most have been exceeded by a considerable amount. This has made the prototype oxygen sensor capable of being used to make in-situ measurements during field testing in a waste-water management plant. The initial phase of this field testing is described in Section 5.6.

## 5.4 Sensor Response and Performance Parameters

### 5.4.1 Sensor Response

For laboratory testing the probe was immersed in a Lauda RE104 constant temperature bath at 20°C and calculated oxygen and nitrogen gas mixtures were dissolved in the water surrounding the probe using mass flow controllers (Model UFC-1130Unit Instruments, Dublin). The gas flow rate was optimised to minimise the occurrence of air bubbles. A LabVIEW program controlled the gas mixing system. A typical sensor response curve, $\phi$ as a function of oxygen concentration, is shown in Figure 5.2. It is clear that the response displays a good signal-to-noise ratio (SNR) and good repeatability. The repeatability is further illustrated in Figure 5.3. Here the

response, shown as a Stern-Volmer plot, for a particular film over a three-month period is shown. The overlapping data indicate the stability of the response. These data, and the data shown in Figure 5.2, were recorded at 20°C.

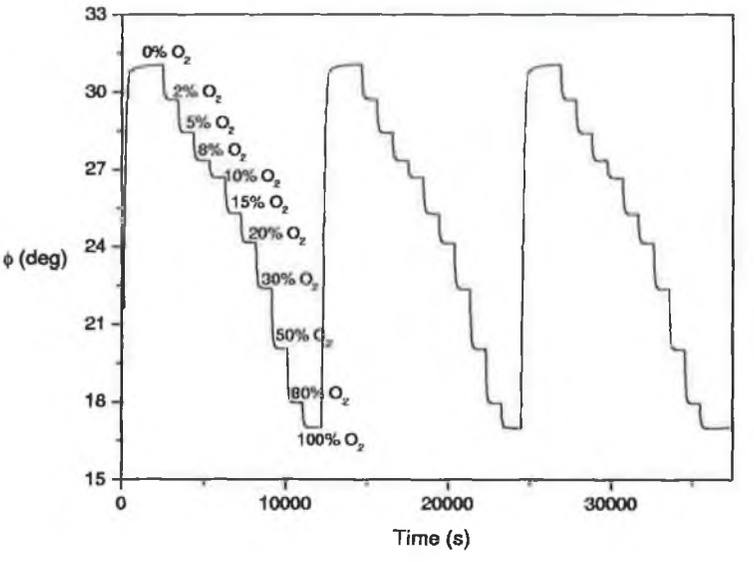


**Figure 5.2:** Plot of Typical Sensor Response to Changing Oxygen Concentration.

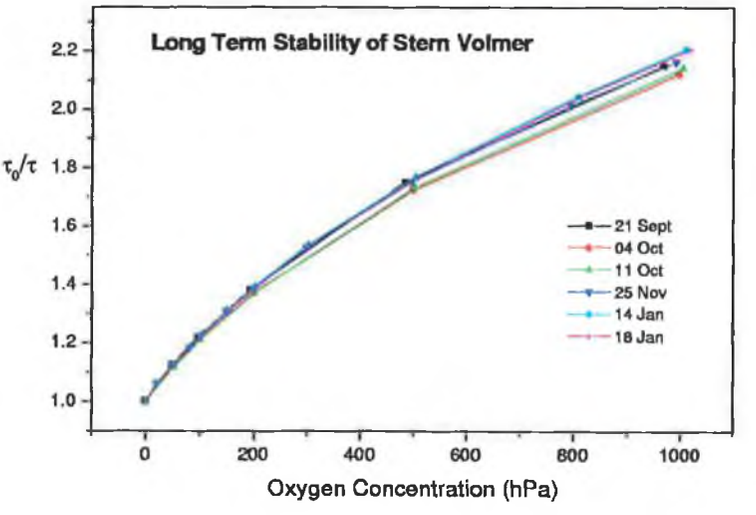


**Figure 5.3:** Overlay of Stern-Volmer curves for a film measured over a 3-month period.

It is clear from Figure 5.2 and 5.3 that the oxygen response is non-linear, especially at low oxygen concentrations where the sensitivity is at its highest. This is particularly obvious in Figure 5.3, the Stern-Volmer plots, where the ideal response would be a straight line. This non-linearity in the Stern-Volmer plot is a result of the existence of a range of quenching environments in the film. This is a consequence of the amorphous nature of the film and is commonly observed for both sol-gel and polymer films[5, 6, 7]. For the waste-water application, higher sensitivity at lower oxygen concentrations is an obvious advantage.

### 5.4.2 Temperature and Pressure Correction

As discussed in Section 2.7 there are a number of contributions to the temperature dependence of the oxygen sensor. The dual LED referencing system, coupled with the fact that the LEDs were selected to have matching temperature characteristics, has referenced any temperature dependence of the phase-measuring electronics out. The resulting baseline temperature coefficient is 0.00087° of phase per °C [8]. There remains a temperature dependence of the ruthenium fluorescence and that of the quenching mechanism. The variation of the response with temperature is shown in Figure 5.4. This shows the sensor response at 5°C and 30°C. Clearly temperature compensation is required for the correct calibration of this sensor. This was achieved by measuring the sensor response as a function of temperature. Measurements were made in the range $5 - 30$°C in steps of 2.5°C. The data was analysed as detailed in Section 5.4.4 in order to produce a temperature correction look-up table.

As mentioned previously, ambient pressure is recorded as well as the phase value corresponding to the oxygen concentration and the ambient temperature reading. The pressure reading is recorded in units of hecto-pascals (hPa) and is written to the output data file. The oxygen concentration is converted to the correct partial pressure value by Equation 5.1.

$$hPa = [(P - P_{VP})\frac{[O_2]}{100}] \qquad (5.1)$$

Here $P_{VP}$ is the vapour pressure of the water, which is 25hPa at 20°C.

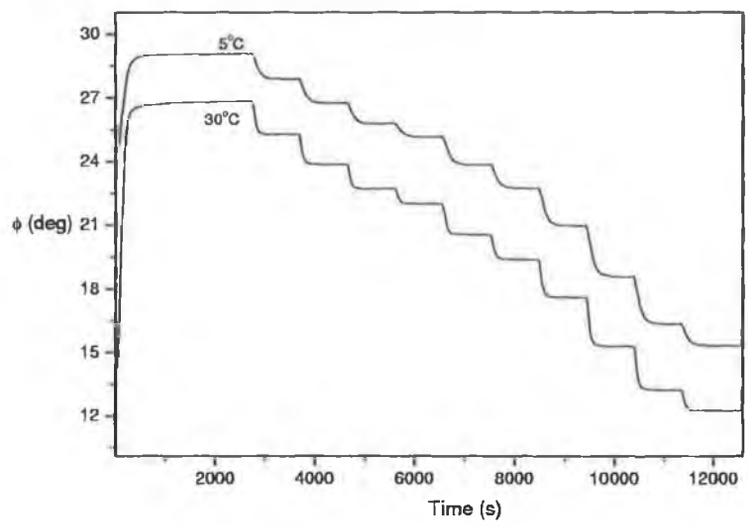


**Figure 5.4:** Plot of Typical Sensor Response to Changing Oxygen Concentration at Different Temperatures.

### 5.4.3 Sensor Performance

As stated previously, the sensor response displays a good SNR. This results in a very low limit of detection (LOD). The LOD and resolution of the sensor were measured as three times the standard deviation of the noise, while averaging for 30 seconds. Because of the non-linearity of the response, the resolution varies with oxygen concentration. The LOD and resolution values for the sensor are given in Table 5.1. It is clear that the LOD value comes well within the specified value (¡10ppb) for the waste-water application. The intrinsic response of the sensor in gas phase is $< 15$ seconds. In this system, the response time is limited by the thickness of the black optical isolation layer. This is not an issue in the current waste-water application. Long-term stability studies have been carried out on a number of sensor films, one of which has been in continuous use for over 18 months.

## 5.5 Calibration Protocol

This section deals with the development of a calibration protocol for the sensor, which would enable the user to obtain a readout of oxygen partial pressure or concentration from a measured phase angle value and ambient pressure and temperature

readings. Each disc has a slightly different response, as seen in Figure 5.5. This necessitates that individual calibration curves need to be generated for each sensor disc.

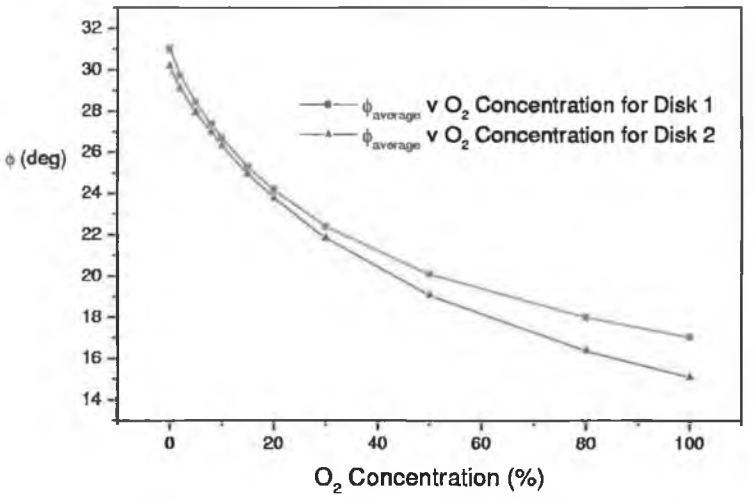


**Figure 5.5:** Variation of Response between Sensor Discs.

The approach used here is to develop a look-up table generated from data consisting of $\phi$ as a function of oxygen concentration, for the temperature range $5 - 30^{o}$C. This section details the data reduction strategies used to generate an appropriate response curve as well as the curve fitting strategies used to generate the look-up table.

### 5.5.1 Data Reduction and Data Format

The raw oxygen calibration data from the sensor film is in the form of Figure 5.2. This data was reduced to a response curve similar to that shown in Figure 5.5 by averaging over each horizontal step in Figure 5.2 to give a single $\phi_{ave}$ value for each oxygen concentration value. This was done using an automated data-averaging program, DataAve (see Appendix II) written in LabTalk[9], the in-built programming language of the Microcal Origin data analysis package[10]. The program differentiates the response shown in Figure 5.2. This identifies the 'concentration steps'. An average $\phi$ value is found for each of these 'concentration steps', and the result is similar to the response plot shown in Figure 5.5 of $\phi_{ave}$ v $[O_2]$. These data then

need to be fitted to generate a look-up table. The limitation here is that there are only a finite number of data points. Any curve fitting routine must produce a good fit in between these data points that accurately models the behaviour of the sensor film. Prior to curve fitting to the data set, a number of different data formats were investigated.

$\underline{\phi_{ave} \text{ v } [O_2]}$ This format is as in Figure 5.5 and is obtained directly from the raw data as explained earlier. Figure 5.6 shows the response as a function of temperature. The variation can be clearly discerned using this data format and this was the format chosen for use in the calibration protocol of the sensor.

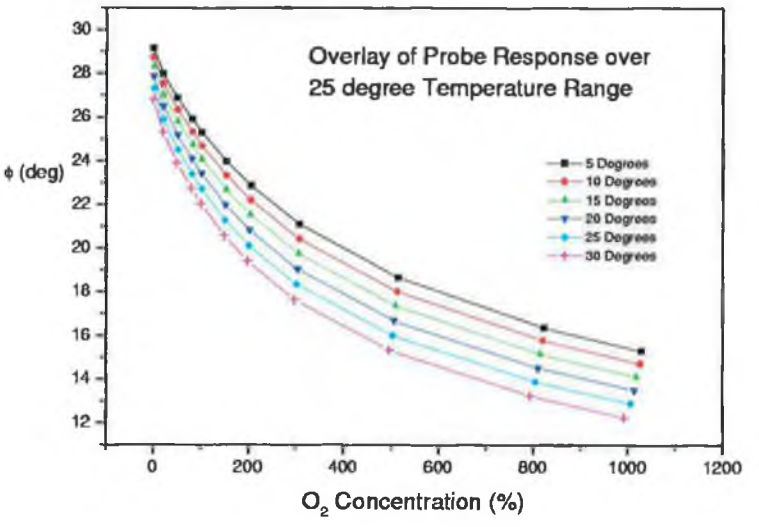


**Figure 5.6:** Variation of Sensor Response with Temperature.

$\underline{d\phi_{ave}/d[O_2]. \text{ v } [O_2]}$ This format is shown in Figure 5.7. While this format highlights the high sensitivity area at low oxygen concentrations there was a persistent discontinuity in the region between $0 - 2\%$ which made curve fitting to this data format complicated.

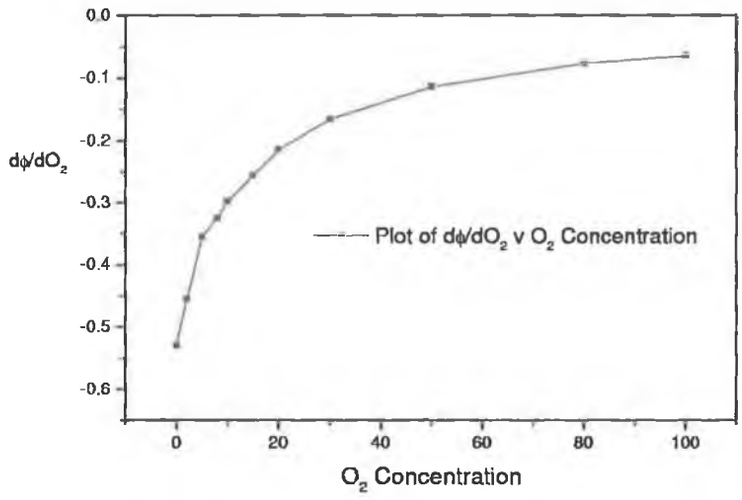


**Figure 5.7:** Plot of $d\phi_{ave}/dO_2$ v Oxygen Concentration.

**The Stern-Volmer representation** of the sensor response data was also considered. Figure 5.8 shows the temperature variation of Figure 5.6 expressed in Stern-Volmer format. Clearly this compressed the data, particularly at low oxygen concentrations and so would not be suitable for the generation of a look-up table.

Overall the $\phi_{ave}$ v $[O_2]$ data format was considered most suitable and was used subsequently for curve fitting and for the generation of the look-up table.

## 5.5.2 Curve Fitting Strategies

Three different curve fitting approaches were tried and evaluated. They are summarised in this section.

### 5.5.2.1 Microcal Origin

This used the Non-Linear Curve Fitting option in the Microcal Origin computer package [10]. It allows an equation to be entered externally as the basis for fitting a curve to the data points. The equation used was of the form:

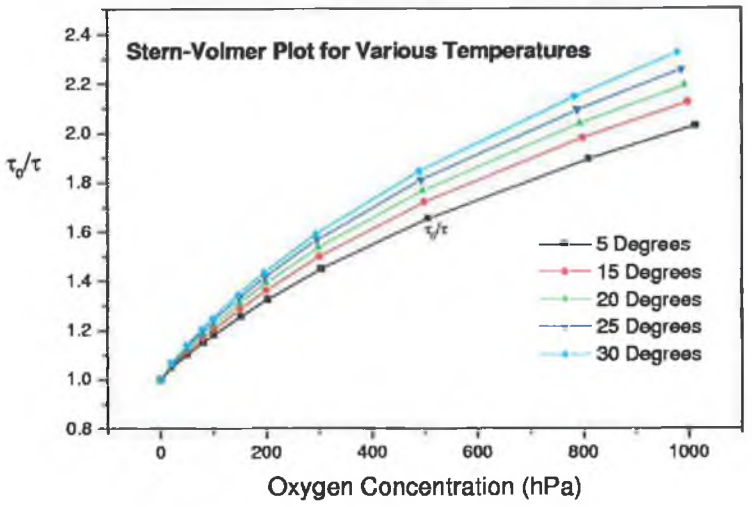


**Figure 5.8:** Variation of Stern-Volmer Plot for Various Temperatures.

$$y = y_0[\frac{A}{1+Bx} + (1-A)] \qquad (5.2)$$

The equation was first solved to give estimates for A and B. These values were then entered into Origin and better estimates were generated by the computer package. Since the equation initially had to be solved manually this method proved to be very tedious. It did however produce a data set which was an improvement on the small number of measured data points.

#### 5.5.2.2 Polynomial Fitting

A Fortran computer program was used to fit a polynomial to the data in this approach, up to a third order fit. The degree of the polynomial can be any number up to one less than the number of data points in the data set. An output file of 100 data points is generated. An example of the fit is shown in Figure 5.9

While the fit is good at low oxygen concentrations, it is very unsatisfactory at

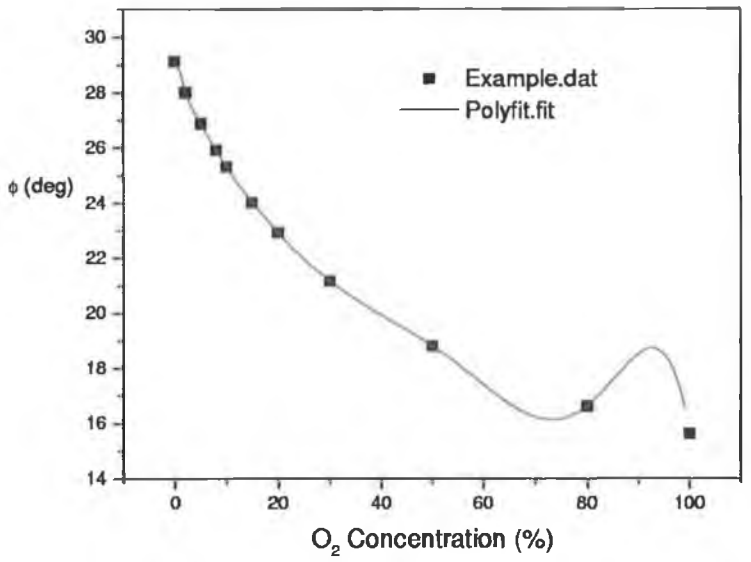


**Figure 5.9:** Plot of Fit Achieved using Polyfit.exe and Original Data.

higher concentrations. Improved fits were obtained when scaling was introduced into the computer program. This involved compressing the data along the x-axis and rescaling after the fit was generated. The strategy here was to reduce the distance between the data points. Figure 5.10 shows the resultant fit for (a) square-root scaling and (b) logarithmic scaling. Although the logarithmic scaling produced a better fit to the data, neither method produced an acceptable calibration curve. The code for the Fortran computer programs used is listed in Appendix III.

#### 5.5.2.3 Cubic Spline Fitting

This method produced a satisfactory fit to the data and was used to generate the calibration look-up table. It involves grouping the data points into sets of adjacent points and fitting each set separately with a cubic polynomial. The form of the polynomial is given in Equation 5.3.

$$y_i(x) = a + b_i x + c_i x^2 + d_i x^3 \qquad (5.3)$$

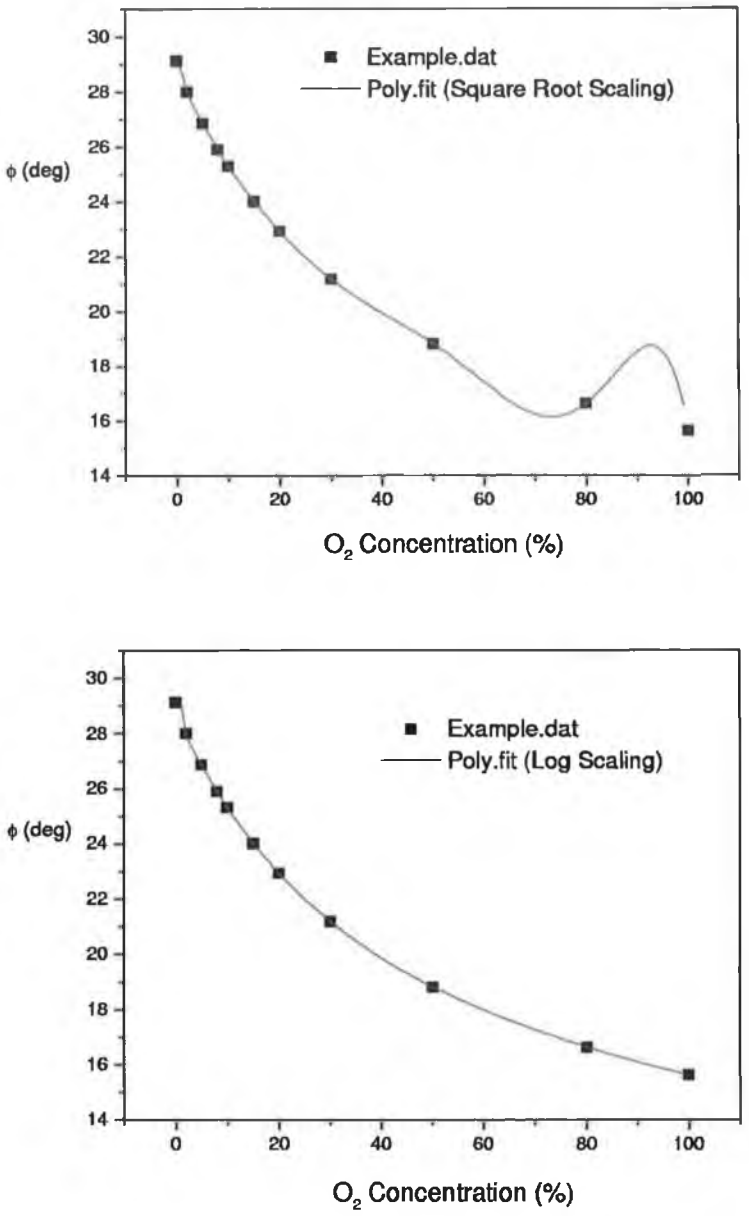


**Figure 5.10:** (a) Plot of Fit Achieved using Poly.exe with Square Root Scaling; (b) Plot of Fit Achieved using Poly.exe with Square Root Scaling.

where the interval being considered is: $x_i \leq x \leq x_{i+1}$

There is also a condition that the first derivative of the polynomials be equal at the common point between two intervals. This results in a smooth curve that is a good fit to the data. The program has the ability to handle multiple files, and it

allows the user to extract an unknown oxygen concentration by inputting a phase and temperature value. Each of the temperature curves in Figure 5.6 were spline fitted, enabling the generation of a 3-dimensional look-up table. The data from this table is shown in the 3-dimensional plot in Figure 5.11. Again the code for the Fortran computer program associated with this cubic spline fitting program can be found listed in Appendix IV.

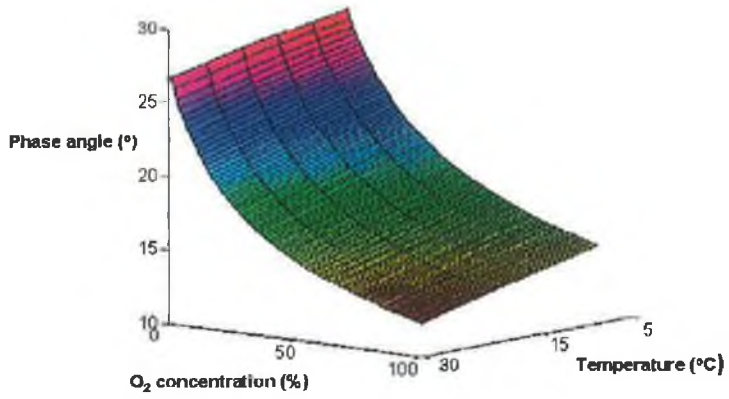


**Figure 5.11:** Calibration Curve for DO Probe.

The author of this thesis is indebted to Dr. Tony Cafolla, School of Physical Sciences, Dublin City University, for providing the two Fortran computer programs used in this analysis.

## 5.6 Initial Field Testing

Initial field testing of this sensor system took place between April and September 1999. The system was installed at a waste-water treatment plant in the UK. A set-up similar to that shown below was created at the plant. The probe head was mounted on a long pole (alongside the existing Clark electrode oxygen sensor that is used at the plant) and immersed in the waste-water. Connections were made to the control unit of the system which was housed in a weather-proof box. Extended cables were used for this as the pole length was approximately 3m. Further extended

cables were used to connect the control unit of the system to the data acquisition computer stored in a mobile trailer parked close to the control unit. Using a modem the data could be retrieved from DCU.

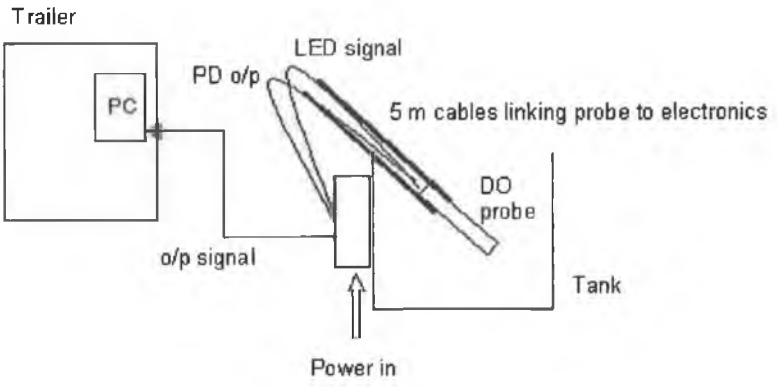


**Figure 5.12:** Phase 1 Field Testing Set-up.

Unfortunately problems arose with regard to interfacing the probe output to the waste-water company computer systems. Also prolonged immersion of the aluminium probe head in the waste-water caused severe corrosion of the metal. It was assumed that this corrosion was due to the extremely harsh environment in which the probe was placed. Also consultation with experienced engineers in the waste-water industry indicated that aluminium was not an ideal material for the probe housing to be manufactured from. Because of this degradation of the metal water began to leak into the probe head and damage the electronic and optoelectronic components inside the probe head. Consequently no useful data was obtained. The modifications that were made to the design of the prototype based on this experience are detailed in the next section. A photograph of the sensor probe in operation in the waste-water treatment plant is shown in Figure 5.13. It shows the harsh environment that the sensor has to operate in.

## 5.7 Modifications Based on the Field Testing Results

After the sensor system was retrieved from the site of the field testing an investigation was carried out to find the reasons for the failure of the field test. Improvements were made to the output wiring to facilitate compatibility of the sensor with plant

**Figure 5.13:** Phase 1 Field Testing of DO Waste-Water Monitoring Probe.

systems. However it was obvious that even if the sensor had operated correctly for a period of time it would have failed after the corrosion of the aluminium casing and the leakage of the water.

It was decided that the casing material would have to be changed to some material that would not corrode. Plastic was chosen as the new casing material due to its relatively inexpensive cost, the ease with which it can be machined and its resistance to corrosion. In particular Poly Vinyl Chloride(PVC) was chosen as the material for the manufacture of the new casing. A PVC probe head casing was manufactured and the electronic and optoelectronic components mounted inside it as they had been in the aluminium casing. This solved the corrosion and leakage problem, but presented some problems of its own.

The high impedance electronic components included in the probe head had previously been electrically shielded by the aluminium casing. This metal casing also provided a ground for the circuitry. However the new plastic casing did not serve this purpose due to the fact that PVC is an electrical insulator. As a result, the scans of varying oxygen concentrations used to characterize the sensor(scans similar to those in Figures 5.2 and 5.4) were affected by drift and were not repeatable. These problems had to be eliminated before the sensor could reach the level of accuracy it had previously achieved in the aluminium casing, and before it could be returned to the waste-water monitoring plant for the second phase of field testing.

These improvements involved shielding both the electronic and optoelectronic components contained within the PVC probe head. This was done by lining parts of the inside surface of the probe head with silver paint and connecting this silver paint to the ground line of the circuit using a copper wire. Copper tape was also used to shield the electronic circuitry and protect it from electrostatic charges that may have impinged on the performance of the sensor. These improvements yielded response plots that were free of drift, repeatable and comparable with those obtained using the aluminium casing.

## 5.8 Summary

This chapter has presented the results of the laboratory testing carried out on the waste-water monitoring probe. The specifications of the probe outlined by the industrial partner on this project were given and compared well with the sensor performance in the laboratory. The calibration protocol designed for this sensor system has been described in detail, including data reduction, curve fitting and temperature and pressure compensation.

Finally the initial phase of field testing undertaken using this probe has been described. The set-up used and the small changes that were needed to install the sensor in the harsh environment of a waste-water plant are detailed. Modifications that were made to the sensor system upon retrieval from the field testing site are given and explained.

The probe has now been handed over to another researcher who will implement the second phase of field testing.

# Bibliography


[1] A.K. McEvoy. *Development of an Optical Sol-Gel-Based Dissolved Oxygen Sensor.* PhD thesis, School of Physical Sciences, Dublin City University, 1995. Unpublished.

[2] V. I. Ogurtsov and D. B. Papkovsky. Selection of modulation frequency of excitation for luminescence lifetime-based oxygen sensors. *Sens and Act B*, 51:377–381, 1998.

[3] A. McEvoy, C. McDonagh, and B. D. MacCraith. Phase-fluorimetric dissolved oxygen sensor. *Analyst*, 121:785–789, 1996.

[4] G. O'Keeffe. *Development of Fibre-Optic Evanescent Wave Fluorescence-Based Sensors.* PhD thesis, School of Physical Sciences, Dublin City University, 1995. Unpublished.

[5] A. Mills. Controlling the sensitivity of optical oxygen sensors. *Sens and Act B*, 51:60–68, 1998.

[6] A. Mills. Optical sensors for oxygen: A log-gaussian multisite-quenching model. *Sens and Act B*, 51:69–76, 1998.

[7] E.R. Carraway, J.N. Demas, B.A. DeGraff, and J.R. Bacon. Photophysics and photochemistry of oxygen sensors based on luminescent transition-metal complexes. *Analytical Chemistry*, 63:337–342, 1991.

[8] C. Kolle. Development of an optical dissolved oxygen sensor. *Unpublished, School of Physical Sciences, Dublin City University*, 1999.

[9] Ltd. Microcal Software. *Microcal LabTalk User Manual; Version 6.* 1999.

[10] Ltd. Microcal Software. *Microcal Origin User Manual; Version 6.* 1999.

# Chapter 6

# Porphyrin-Based Oxygen-Sensitive Films

## 6.1 Introduction

In the past, a large proportion of optical oxygen sensor research has involved transition metal complexes such as $[Ru(Ph_2phen)_3]^{2+}$ [1, 2, 3]. However in recent years a large amount of research has taken place with the aim of developing optical oxygen sensors using metallo-porphyrins as the entrapped indicator dye. This family of oxygen-sensitive complexes had previously proven to be optically unstable. However the emergence of newer forms of these metallo-porphyrins, with more stable optical characteristics, has revived the interest into their use in oxygen sensor systems. The major advantage of porphyrin complexes over ruthenium complexes is the longer lifetime of the complex, and hence its greater sensitivity to oxygen. These complexes are also less temperature sensitive than their ruthenium counterparts.

The majority of these metallo-porphyrin-based optical oxygen sensors use a polymer-based film as the support matrix for the indicator dye[4, 5]. Very few sensor systems have reported the use of sol-gel thin films as the support matrix. Those that have, have only reported short-term results and have not presented long-term studies[6, 7]. The aim of this work is to successfully entrap the metallo-porphyrin, Platinum Octoethylporphyrin keytone(PtOEPk), in a sol-gel support matrix, and achieve a sensor performance that is comparable to the best polymer-based PtOEPk optical oxygen sensors reported[4, 5]. Porphyrin-doped sol-gel films would combine the high oxygen sensitivity of the porphyrin with the many advantages of the sol-gel matrix, as discussed in Section 3.2.

## 6.2 Advantages of Porphyrin Complexes for Oxygen Sensing

In general terms, oxygen-sensitive porphyrin complexes have a greater overall response to changing oxygen concentration than other complexes used in oxygen sensor systems. In particular, this is the case between the PtOEPk and $[Ru(Ph_2phen)_3]^{2+}$ complexes used throughout this work, and this is as a result of the longer fluorescence lifetime, $\tau$, of the porphyrin($60\mu$s for the complex used here) described by Equation 2.3, the Stern-Volmer equation. As can be seen from Figure 6.1 the greater response to changing oxygen is most pronounced at lower oxygen concentration levels. The data used to generate this plot was collected during laboratory experiments.

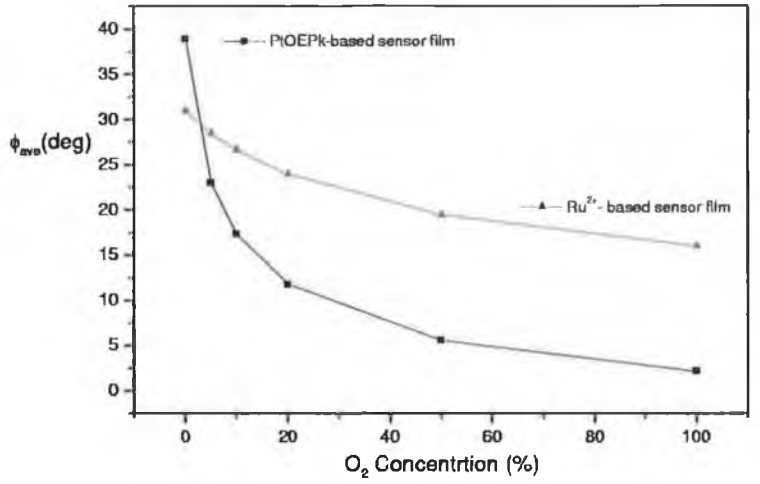


**Figure 6.1:** Plot of $\phi_{ave}$ v $O_2$ concentration for PtOEPk and $[Ru(Ph_2phen)_3]^{2+}$ films in gas phase.

A Stern-Volmer plot of a PtOEPk oxygen sensor film, Figure 6.2, shows a high degree of non-linearity compared to the ideal linear case shown in Figure 2.5. This is a consequence of the way in which the microscopic environment of the complex in the matrix varies for different porphyrin molecules. Again, the data used to generate this plot was collected during laboratory experiments.

For applications that generally operate at the low oxygen concentration levels these PtOEPk-based films are more advantageous, due to their high sensitivity in this area. An example of such an application is the waste-water industry, and in particular the waste-water monitoring probe described previously in Chapter 5. Such

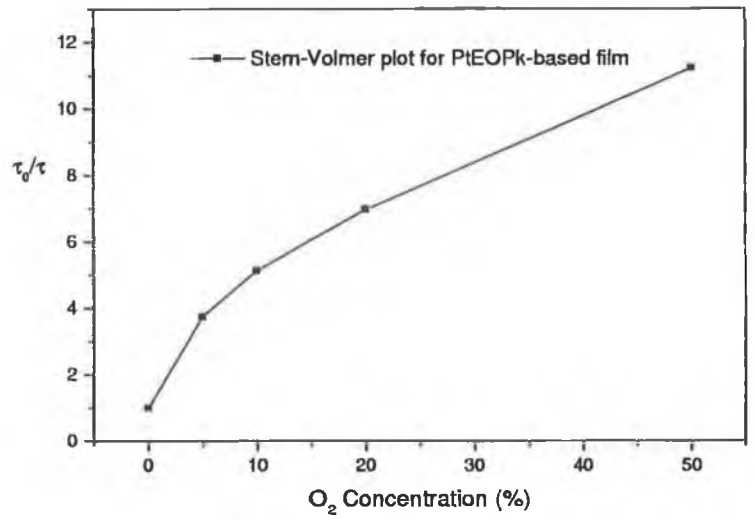


**Figure 6.2:** Stern-Volmer plot for PtOEPk-based film in gas phase.

a probe, designed with PtEOPk entrapped in the sol-gel matrix, would provide a lower limit of detection(LOD) and make the sensor system more sensitive at lower concentrations.

## 6.3 Description and Evaluation of Commercial Porphyrin Oxygen System

A commercial system was purchased for initial characterisation of the porphyrin-doped sensor films[8]. A dedicated probe would be designed when the optimum films were identified.

### 6.3.1 Fibre-Based Porphyrin Sensor System

A schematic of the commercial fibre-based system was drawn and is shown in Figure 6.3.

Light from a yellow excitation LED of $\lambda = 590$nm (TLYH180P, Toshiba, Japan) (see Figure 2.5 for the absorption bands of the porphyrin) which is contained within the sensor unit, is transmitted down the optical fibre and is incident on the sensor film. The launch end of the fibre is inserted into the unit and is positioned as close as possible to the yellow excitation LED.

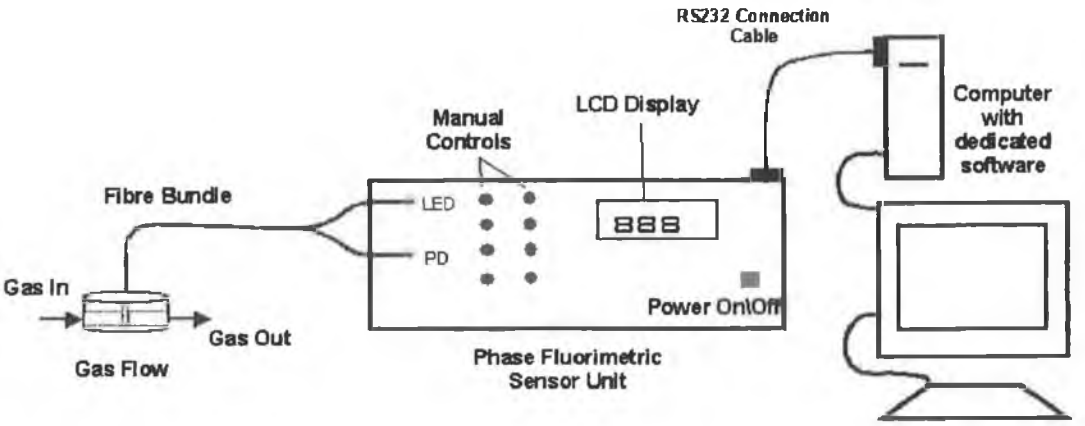


**Figure 6.3:** Schematic diagram of fibre-based sensor system.

The phosphorescent light from the excited PtOEPk-doped sensor films($\lambda$ = 751nm) is transmitted back up the fibre and through the second leg of the bifurcated fibre bundle. This phosphorescent light is then detected by a photodiode, which, like the excitation LED, is contained within the sensor unit. A bandpass optical filter with its peak transmission at 590nm(the excitation wavelength of the PtOEPk complex and the peak emission wavelength of the yellow LED) is placed in front of the yellow LED to ensure that only this yellow excitation light is launched into the fibre bundle. A second optical filter, a Schott Glass RG9 interference filter, is placed in front of the photodiode detector. This is to ensure that only the phosphorescent light from the excited sensor films is detected and that no stray light from the yellow LED is detected. A second LED, used as a reference LED, is also contained within the sensor unit. This LED has its peak emission wavelength in the near-infrared, at 700nm. It is placed in close proximity to the photodiode detector and its light is passed by the Schott Glass filter.

The sensing technique used in this fibre-based sensor system is phase fluorometry, the same technique used in the waste-water monitoring probe described in Section 5.2. All the amplification, phase measuring and data processing electronic circuitry involved in this sensing technique are contained within the sensor unit. The output from this sensor unit can be recorded in two different ways. The first is through the use of an analog 10mV output line, which can be connected to a data logger. The second output method, which was the method used during this work, involved connecting the sensor system, via an RS232 cable, to the serial port of a PC. Using the dedicated software supplied with this system, the phase-shift($\phi$), intensity(I)

and temperature(T) data could be viewed on the screen as well as recorded in a data file. The value of the most recent measurement made by the sensor system($\phi$, I or T) can also be seen on the front panel display of the unit.

### 6.3.2 Evaluation of the Operation of the Porphyrin Oxygen Sensor and Typical Results

Supplied with this fibre-based porphyrin oxygen sensing system when purchased were a set of PtOEPk-doped polymer-based sensor films. The performance of these films has previously been reported[9], and it is accepted that their oxygen sensitivity and long-term stability are very good. These proven polymer films were used to characterise this new fibre-based sensor system, and evaluate its performance as an oxygen sensor. The substrate used for these films was a white reflecting filter paper. The relevance of this was discussed in Section 3.5.

This system was characterised using a method similar to the method developed for calibrating the DO waste-water monitoring probe, and detailed in Section 5.5. A plot of varying oxygen concentration versus time for several of these polymer sensor films was generated. These plots, similar to those shown in Figure 6.4 were examined for signal-to-noise ratios(SNR), oxygen sensitivity, repeatability from cycle to cycle, and repeatability between sensor films.

A measurement range of approximately $35^o$ of phase was achieved for all of these polymeric sensor films. This compares with a value of $15^o$ of phase that is achieved with the $[Ru(Ph_2phen)_3]^{2+}$-based sensor system described in Chapter 5. This phase difference reflects the difference in sensitivity of the complexes mentioned previously. The repeatability of these scans from cycle to cycle was excellent, as can be seen from Figure 6.4, which shows excellent stability with time and also excellent repeatability. The repeatability between different sensor films, from the same PtOEPk cocktail batch, was also excellent, proving to be better than that of different $[Ru(Ph_2phen)_3]^{2+}$-based sensor films, characterised in Chapter 5.

Figure 6.5 shows some stability tests that were carried out on this sensor system. For these experiments the sensor system was run continually for an extended period of time, while the oxygen concentration was kept constant. This was performed at several different oxygen concentration levels so as to investigate the change in SNR as the phosphorescent light levels from the sensor films varied.

As can be seen from this plot the fibre-based sensor system is very stable over

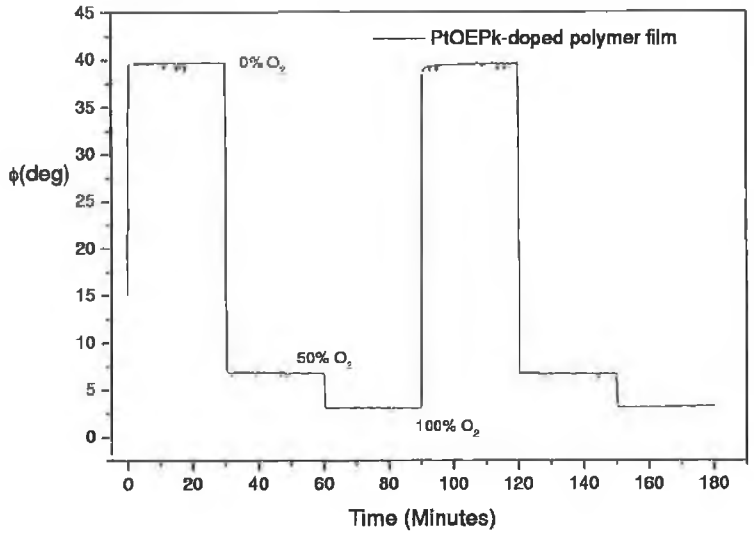


**Figure 6.4:** Plot of $\phi$ v time for PtOEPk polymer-based sensor film.

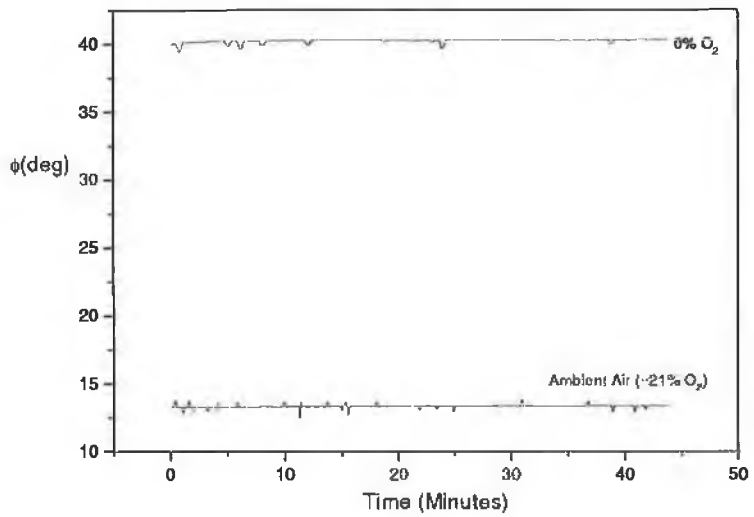


**Figure 6.5:** Plot of the stability of the $O_2$ response of the fibre-based sensor system with time.

extended periods of time and the SNR produced at all the tested concentration levels are acceptable. At $0\%O_2$ the SNR was approximatley 106, while at ambient air ( $21\%O_2$) the SNr reduced to approximately 40.

The fibre-based porphyrin oxygen sensor system evaluated here performed very

well and produced results that indicated that it is a good tool for use in characterising PtOEPk-doped sensor films. The experiments carried out during this evaluation produced results that agreed very well with the specifications provided by the manufacturer. The few small drawbacks associated with this system can be overcome in a laboratory environment and do not affect the systems ability to characterise porphyrin sensor films. These drawbacks include losses or changes in signal due to imperfections or bends in the fibre bundle, inefficiencies in the launching of the excitation light into the fibre and detection of the emitted light at the photodiode due to fibre-end insertion variations and problems with the serial connection to the PC.

## 6.4 Oxygen Sensing with Porphyrin-Doped Sol-Gel-Type Films

As discussed in Section 3.4, PtOEPk was entrapped in several different support matrices in an effort to establish the optimum support matrix for its use as an optical oxygen sensor. Various sol-gel formulations, a soluble ormosil formulation as well as a polymer ethyl cellulose method are described. All of the sensor films fabricated using PtOEPk as the entrapped oxygen-sensitive complex were tested in the same way using the fibre-based system described in both this chapter and also in Chapter 4. As previously stated the method used to examine these new types of sensor films was similar to that used to characterise the PtOEPk polymer-based films supplied with the fibre-based system, and used to calibrate the $[Ru(Ph_2phen)_3]^{2+}$-based DO waste-water monitoring probe detailed in the previous chapter. In all the examples, better results were obtained for those sensor films coated on the white Millipore filter paper substrate, described in detail elsewhere[9], rather than on the transparent acetate substrate. This is a result of the design of the fibre-system and obviously proved a limitation in this work as it restricted the choice of substrate.

### 6.4.1 Porphyrin-Doped Sol-Gel Films

Several different formulations of sol-gel matrices were investigated for use with PtOEPk as optical oxygen sensors. The differences between each of these sol-gel formulations have previously been described in detail in Chapter 3, and the reasons for their use have been given. All of these sol-gel formulations with PtOEPk en-

trapped were coated onto both transparent acetate substrates and white Millipore filter paper substrates, with the latter providing the better results. It is mainly these results that are presented here.

For three of the sol-gel matrix types described above(TEOS, MTEOS and TESPIC) plots of phase-shift($\phi$) versus time(t) are given. Figure 6.6 shows these plots for sensor films coated on a transparent substrate. It is obvious from the very low signal levels at high oxygen concentrations, and the low SNR throughout this plot, that sensor films coated on this type of substrate are not suitable for use as optical oxygen sensors with the fibre system.

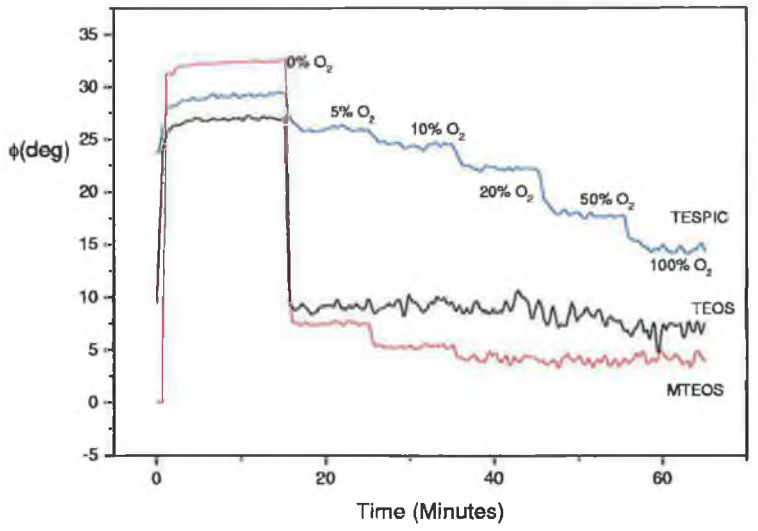


**Figure 6.6:** Plot of $\phi$ v time for sol-gel-doped PtOEPk films coated on transparent acetate substrates.

On the other hand, Figure 6.7 shows the same type of plot($\phi$ v t) for PtOEPk-doped sol-gel films coated on the white Millipore filter paper substrate. As can be seen from these plots the SNR throughout the range of oxygen concentrations is higher than for those in Figure 6.6, as are the signal levels at the higher oxygen concentrations. Hence all formulations were coated on this substrate for characterisation purposes.

It is clear that TEOS-based sensor films do not have a satisfactory response, and hence this sol-gel matrix formulation was discontinued as a support matrix for PtOEPk-based sensor films.

The results obtained from MTEOS- and TESPIC-based sensor films are com-

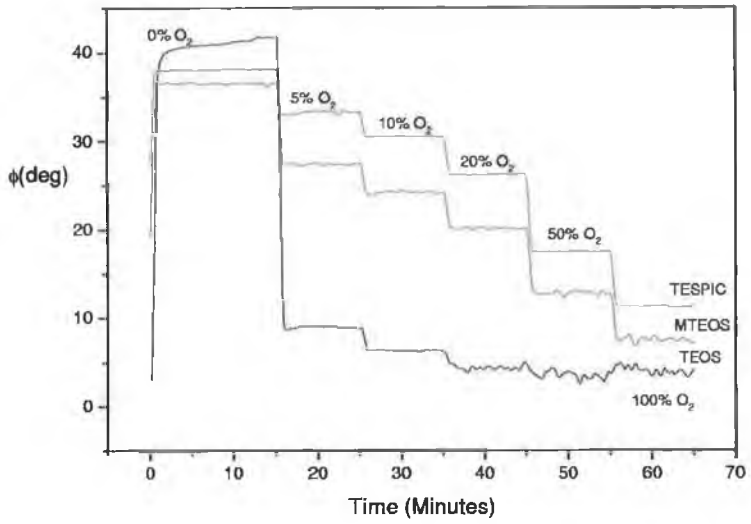


**Figure 6.7:** Plot of $\phi$ v time for sol-gel-doped PtOEPk films coated on white Millipore filter paper substrates.

parable, in both signal level($\phi$ value) and SNR, to the established polymer-based films used to evaluate the fibre-based system in Section 6.3 above. Figure 6.8 shows the oxygen response for the three films. Clearly the polymer film still has greater sensitivity.

Further investigation of the use of these sol-gel formulations as support matrices for oxygen sensing is discussed in the next section and in the following chapter.

### 6.4.2 PtOEPk-Doped Soluble Ormosil Films

A soluble ormosil support matrix method was investigated as an alternative to both sol-gel and polymer support matrices. As discussed in Section 3.4, this formulation produces a hybrid film which is polymer-like, but with many of the advantages of sol-gel films. Again as stated at the beginning of this section, these sensor film types were coated on both transparent and white substrates. As was the case with the sol-gel based sensor films, the results were obtained for those sensor films coated on the white Millipore filter paper substrate. These results for the white filter paper substrate are shown below.

The signal levels at all oxygen concentration levels, as well as the SNR, are comparable, if not better, than those achieved with the sol-gel based sensor films

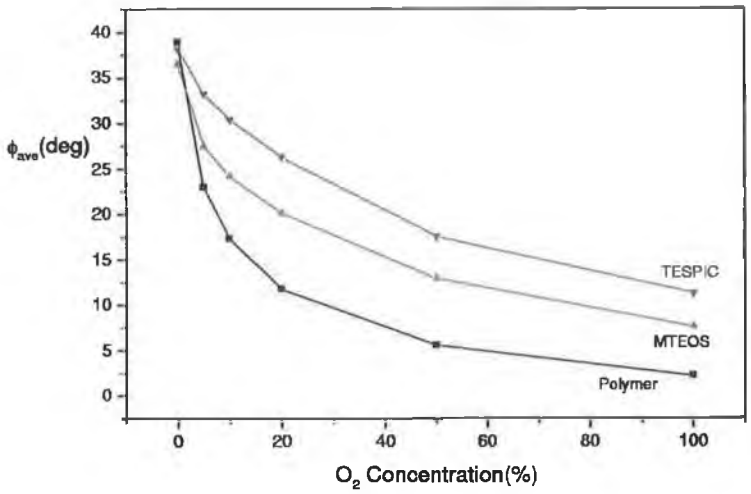


**Figure 6.8:** Plot of $\phi_{ave}$ v $O_2$ Concentration for an MTEOS, a TESPIC and a polymer-based(polystyrene) sensor film.

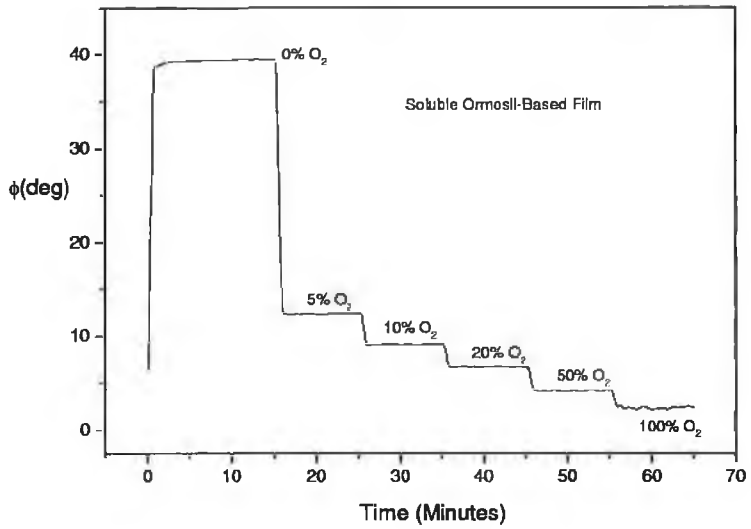


**Figure 6.9:** Plot of $\phi$ v time for a Soluble-Ormosil-doped PtOEPk film coated on a white Millipore filter paper substrate.

described above. These $\phi$ values and SNR values also compare very favourably to those obtained with the polymer-based films used in Section 6.3. One major difference that is apparent is the sensitivity of these soluble ormosil films at low

oxygen concentrations. This very large sensitivity is much greater than that shown above for the sol-gel based sensor films, and has a profound effect on the Stern-Volmer plot of this type of sensor film. This is discussed later in Section 6.5.

### 6.4.3 Porphyrin-Doped Ethyl Cellulose Films

Polymer-based PtOEPk-doped oxygen sensor films were also fabricated during this work. This was done in order to have a direct comparison with the large amount of previously reported polymer-doped PtOEPk work[4, 5]. Investigating films of this type also provides a direct comparison with both the sol-gel and soluble ormosil doped PtOEPk sensor films previously detailed.

The response of these sensor films to oxygen was very good and compared well with those results presented above for other support matrix types, and also with the results of previously reported polymer-based PtOEPk sensors. This response to oxygen is shown below in Figure 6.10, and as can be seen from a comparison with the plot in Figure 6.9, is a very similar response to that of the soluble ormosil based PtOEPk sensor films.

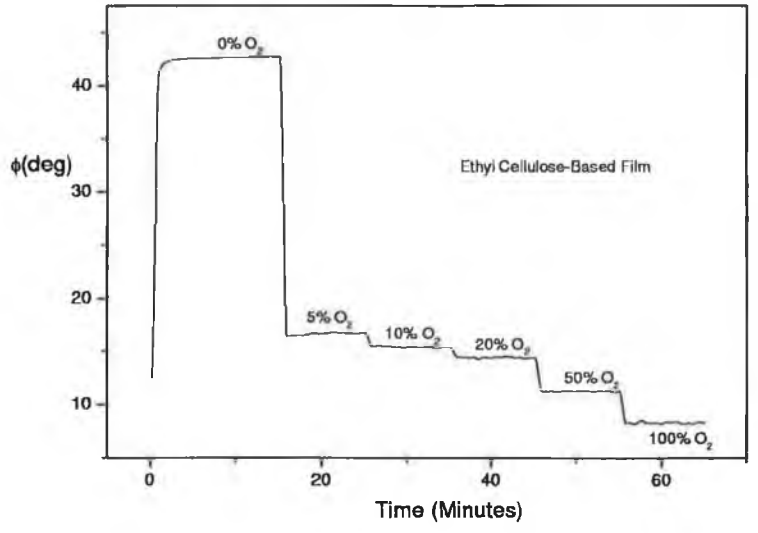


**Figure 6.10:** Plot of $\phi$ v time for an Ethyl-Cellulose-doped PtOEPk film coated on a white Millipore filter paper substrate.

## 6.5 Evaluation of Sol-Gel Films as a Sensor Matrix for Porphyrin Compounds

In this section the results presented for the different support matrices investigated, the various sol-gel formulations, the soluble ormosil films and the polymer-based method are analysed and three are selected for further investigation using both the fibre-based system and also a new modular phase-fluorometric system described in Chapter 7. The reasons for the selection of these particular sensor films are given and justified using the results presented in the previous section.

### 6.5.1 Evaluation of PtOEPk Sensor Film Types

As is clear from the results presented above for the sol-gel-based PtOEPk-doped sensor films, two of the investigated formulations were the only ones that could be used as reliable oxygen sensors. These were the MTEOS- and the TESPIC-based formulations. However the MTEOS-based formulation was deemed to be a better sensor film than the TESPIC-based film. This was due to the excellent long-term stability that the MTEOS-based sensor films exhibited over several weeks. This long-term stability, although it is for a sensor film coated on a transparent acetate substrate, where the SNR levels are poor, is shown in Figure 6.11. Although the sol-gel-based sensor film responses shown above in Figure 6.7 show that the TESPIC-based films have a slightly better SNR at higher oxygen concentration levels than the MTEOS-based films, the SNRs of both sensor film types are almost identical at lower oxygen concentrations. This is the concentration region of interest for the type of application associated with this work, hence MTEOS-based sensor films are a good option for further investigation, especially at oxygen concentrations of less than $30\%O_2$.

It is clear that there are large differences in the oxygen sensitivity between the various sensor film types. This difference in sensitivity is most pronounced at low oxygen concentrations, less than $5\%O_2$. This behaviour is most easily observed in the Stern-Volmer plots of the data, where a high degree of non-linearity is an indication of the high sensitivity at low oxygen concentrations. This ca be seen in Figure 6.12 for MTEOS and Soluble Ormosil films. Since all the films under investigation are amorphous, or glass-like, the porphyrin is entrapped in a range of different environments, producing a range of different lifetimes. This distribution varies from

matrix to matrix. Both soluble ormosil- and ethyl cellulose-based PtOEPk sensor films have large sensitivity at these low oxygen concentrations(approximately $20^o$ of phase). The selected sol-gel-based support matrix, MTEOS, provides sensor films that have a sensitivity of approximately $10^o$ of phase in this area. Although this is not quite as large as that of the other two PtOEPk sensor films reported here, it is still much improved on the $[Ru(Ph_2phen)_3]^{2+}$-based sensor films used in the waste-water monitoring system characterised in Chapter 5. Taking this into account these MTEOS-based sensor PtOEPk sensor films could be used to improve the waste-water sensor described previously in this work. A further improvement may be possible through the use of the soluble ormosil-based films, however the long-term stability of these films has yet to be established.

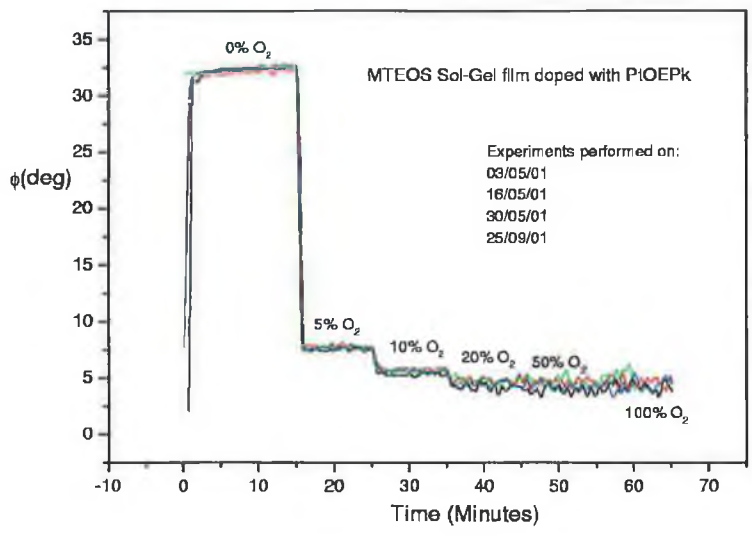


**Figure 6.11:** Long-term stability of the MTEOS-doped PtOEPk sensor film.

### 6.5.2 Optimum Films for Further Investigation

Three of the support matrices investigated for use with PtEOPk as optical oxygen sensors during this work, and whose results are presented above, were chosen for further work and investigation, namely MTEOS, soluble ormosil and ethyl cellulose. These choices were based on the interpretation of the above results, and therefore on the suitability of these PtEOPk-doped support matrices for use as optical oxygen sensors. These support matrices, along with reasons for their selection, and an

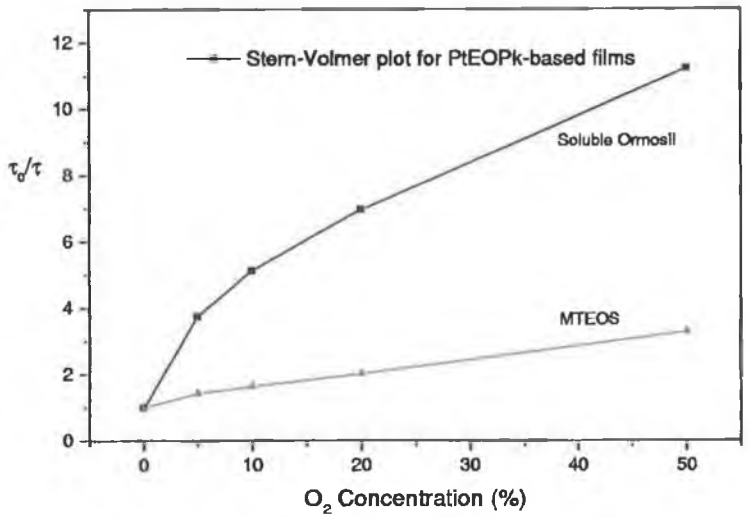


**Figure 6.12:** Stern-Volmer plots for MTEOS-doped and Soluble Ormosil-doped PtOEPk sensor films.

assessment of their performance to date as optical oxygen sensors, are listed in the table below.

| **Support Matrix** | **Oxygen Sensor Characteristics** | **Performance as an Oxygen Sensor** |
|---|---|---|
| MTEOS | Long-term stability - Over a period of several weeks | Average |
| Soluble Ormosil | High sensitivity at low $O_2$ concentrations - 20 Degrees of phase in 5% $O_2$ | Excellent |
| Ethyl Cellulose | High sensitivity at low $O_2$ concentrations 20 Degrees of phase in 5% $O_2$ | Good |

Table 6.1: Characteristics of Sensor Films Chosen for Further Investigation

It is clear from this study that the overall performance of polymer porphyrin films is superior to that of sol-gel porphyrin films. The chemical nature of the sol-gel process makes it difficult to successfully entrap porphyrin compounds. However

some success was achieved in this work with MTEOS-based films. It is possible that further optimisation will produce films of comparable performance to polymer films.

## 6.6 Summary

This chapter has dealt with the oxygen sensing experiments performed using sensor films doped with the oxygen-sensitive porphyrin complex, PtOEPk. These experiments were performed using the fibre-based sensor unit introduced in Chapter 4. Here the operation of this sensor system is described, and an evaluation of its operational performance as an optical oxygen sensing system is provided.

The various PtEOPk-doped sensor films introduced in Section 3.4 are characterised and the results of these characterisation experiments are presented. From these response plots the performance of each individual sensor film type as optical oxygen sensors is assessed. This assessment of sensor performance has allowed three of these PtOEPk-doped sensor films to be selected for further investigation and development.

This further investigation with PtOEPk-doped oxygen sensor films was performed using a newly designed modular phase-fluorometric sensing unit. This sensing unit, and its operation, along with the results are described in Chapter 7.

# Bibliography


[1] C. McDonagh, A.M. Shields, A.K. McEvoy, B.D. MacCraith, and J.F. Gouin. Optical sol-gel based dissolved oxygen sensor: Progress towards a commercial instrument. *Journal of Sol-Gel Sci. and Tech.*, 13:207–211, 1998.

[2] C. McDonagh, C. Kolle, A.K. McEvoy, D.L. Dowling, A.A. Cafolla, S.J. Cullen, , and B.D. MacCraith. Phase fluorometric oxygen sensor. *Sens and Act B*, 74:123–129, 2001.

[3] I. Klimant, F. Ruckruh, G. Liebsch, A. Stangelmayer, and O. S. Wolfbeis. Fast response oxygen micro-optodes based on novel soluble ormosil glasses. *Mikrochimica Acta*, 131:35–46, 1999.

[4] D. B. Papkovsky. New oxygen sensors and their application to biosensing. *Sens and Act B*, 124:695–698, 1999.

[5] D.B. Papkovsky, G.V. Ponomarev, W. Trettnak, and P. O'Leary. Phosphorescent complexes of porphyrin keytones: Optical properties and application to oxygen sensing. *Analytical Chemistry*, 67:4112–4117, 1995.

[6] S. K. Lee and I. Okura. Porphyrin-doped sol-gel glass as a probe for oxygen sensing. *Analytica Chimica Acta*, 342:181–188, 1997.

[7] S. K. Lee and I. Okura. Optical sensor for oxygen using a porphyrin-doped sol-gel glass. *The Analyst*, 122:81–84, 1997.

[8] D. B. Papkovsky.

[9] D. B. Papkovsky, A.N. Ovchinnikov, V.I. Ogurtsov, G.V. Ponomarev, and T. Korpela. Biosensors on the basis of luminescent oxygen sensor: the use of microporous light-scattering support materials. *Sens and Act B*, 51:137–145, 1998.

# Chapter 7

# Testing and Evaluation of a Modular Phase-Fluorometric System

## 7.1 Introduction

This chapter introduces a new phase-fluorometric sensor system which was designed by researchers in the Optical Sensors Laboratory at DCU[1]. The ruthenium and porphyrin sensor films were used to test and evaluate this system. The ultimate goal would be a modular system, which could be easily modified to work with a range of sensor films with differing oxygen sensitivities and spectroscopic characteristics, which could be used as a second generation of the sensor systems described previously in this work.

The ease with which this system can be used to experiment with different types oxygen-sensitive sensor films stems from the modular nature of its design. This system has been designed so that each module can be used either as part of the entire system, or as a small part of another system. Indeed, other modules from other sensor systems, can also be used as a part of this overall system. Here the probe head from the DO waste-water monitoring system described in Chapters 4 and 5 is used in conjunction with the modular system described in this chapter.

## 7.2 Description of Phase-Fluorometric System

The design is based largely on the electronic design of the DO waste-water probe reported already in Section 5.2. This new system was intended to be an improved version of the DO waste-water system, capable of being used in a number of applications, hence the modular design of this new system. It is this flexibility that would allow both $[Ru(Ph_2phen)_3]^{2+}$-based and PtOEPk-based sensor films to be tested with this system.

Figure 7.1 shows a schematic diagram of the system described here. As is shown in this diagram, the various modules of the system are separated from each other(although some, like the LED driving circuit and the phase measuring circuitry, are housed in the same enclosure). This allows for interchangeability with modules from other systems and also increases the ease with which damaged components or circuitry can be located and fixed or replaced.

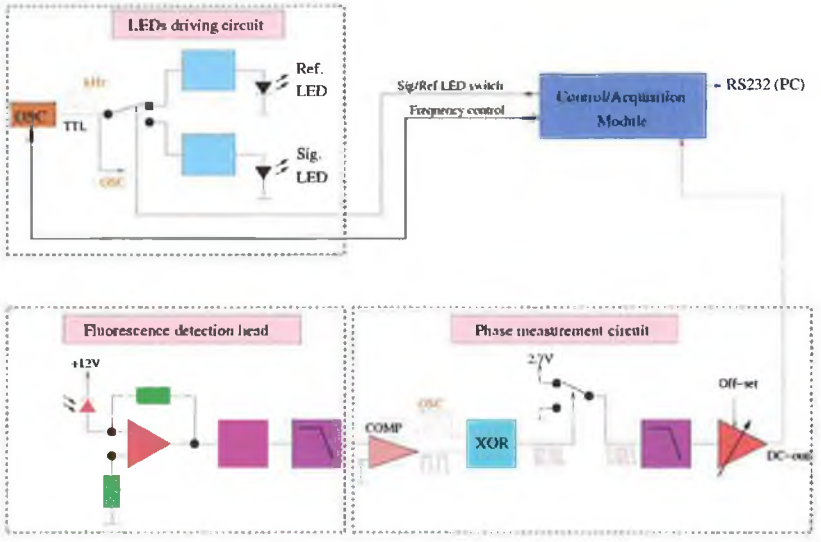


**Figure 7.1:** Schematic of system.

The operation of this system is similar in principle to that of the DO waste-water probe described in earlier chapters. The signal and reference LEDs are modulated at a desired frequency. The light signal from the sensor films is detected by a photodiode and is amplified and filtered before being passed to the phase measuring module. The final output of the system is a d.c. voltage that is proportional to the oxygen concentration level.

The technique used within the phase measuring module to measure the phase-

shift($\phi$), and hence the oxygen concentration level, is the same as that used in the DO waste-water system, that of phase-fluorimetry. This technique has already been described in Section 2.6.

## 7.3 Results for Ruthenium-Based Sensing

Initial testing of this modular phase-fluorometric sensor system was with $[Ru(Ph_2phen)_3]^{2+}$-based sensor films. For this set of sensing experiments the probe head from the DO waste-water system, shown in Figure 4.3, was used as the detection module instead of the fluorescence detection head shown in Figure 7.1. As in the DO waste-water system, the LEDs contained within the probe head were modulated at 20kHz. These $[Ru(Ph_2phen)_3]^{2+}$-based oxygen sensing experiments were firstly performed in gas phase. A new gas flow cell had to be designed for this purpose. It is shown in Figure 7.2.

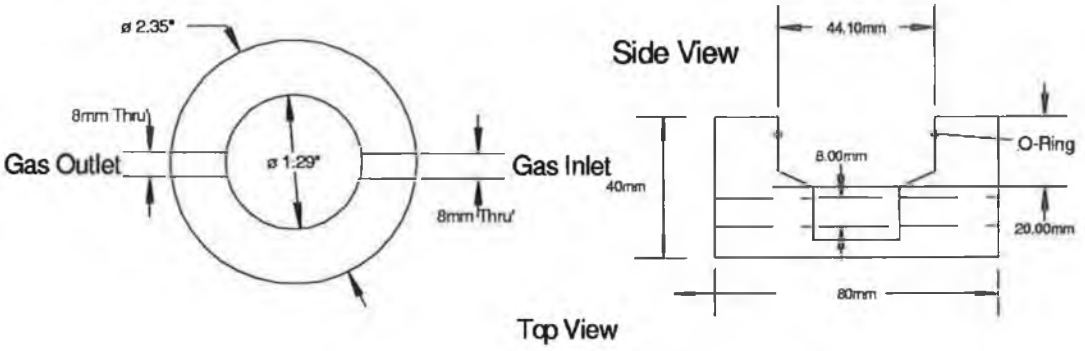


**Figure 7.2:** Schematic of flow cell(gas) for DO probe head.

With the probe head inserted into this new flow cell, it was then connected to the modular system, which in turn had its output connected to a data acquisition PC. This output data was recorded using the same LabVIEW program[2] as was used with the DO waste-water system, described in Chapters 4 and 5. A gas mixture was flowed through the gas flow cell and over the $[Ru(Ph_2phen)_3]^{2+}$ sensor film. This gas mixture was mixed and controlled using the same procedure and equipment as was used for the previous $[Ru(Ph_2phen)_3]^{2+}$ and PtOEPk oxygen sensing experiments. This system is shown in Figure 7.3.

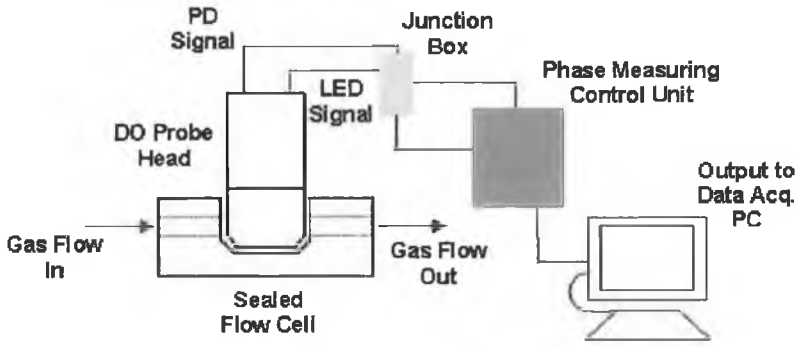


**Figure 7.3:** Schematic of system for Ruthenium-based gas-phase testing.

### 7.3.1 Sensor Response for Ruthenium-Based Films

The sensor response achieved for changing oxygen using the above system was very good. A measurement range of $23^o$ of phase was achieved between 0% and 100% oxygen. This is greater than the measurement range achieved with the DO system as shown in Figure 5.2. However the SNR of this system is lower than that of the previously reported $[Ru(Ph_2phen)_3]^{2|}$-based sensor, as the noise levels have increased along with the signal levels. This is especially evident at higher oxygen concentration levels where the light level emitted from the $[Ru(Ph_2phen)_3]^{2|}$ sensor films is almost fully quenched and of low intensity. The response of the system to changing oxygen is shown in Figure 7.4.

Despite the slight increase in the SNR that is associated with the increase in the measurement range of this response plot, its stability and repeatability over a period of a few weeks is good. The plot in Figure 7.5 shows several cycles from 0% to 100% and back to 0% oxygen. As is clear, the cycle to cycle repeatability is good, eventhough the 100% oxygen phase values are quite noisy.

The inability of the system to stabilise at $0\%O_2$ may have been a characteristic of the sensor film used. This film was more than two years old and may have required a longer time to stabilise at low oxygen concentrations. The repeatable glitch that occurred during the transition between $50\%O_2$ and $100\%O_2$ was thought to be a feature of the measuring electronics, and was due to the small size of the detected signals in this region.

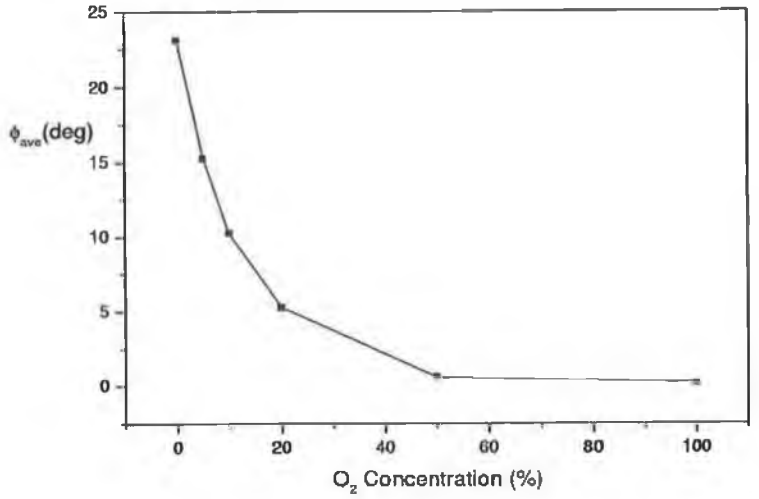


**Figure 7.4:** Response of $\phi_{ave}$ v $O_2$ for Ruthenium-doped film.

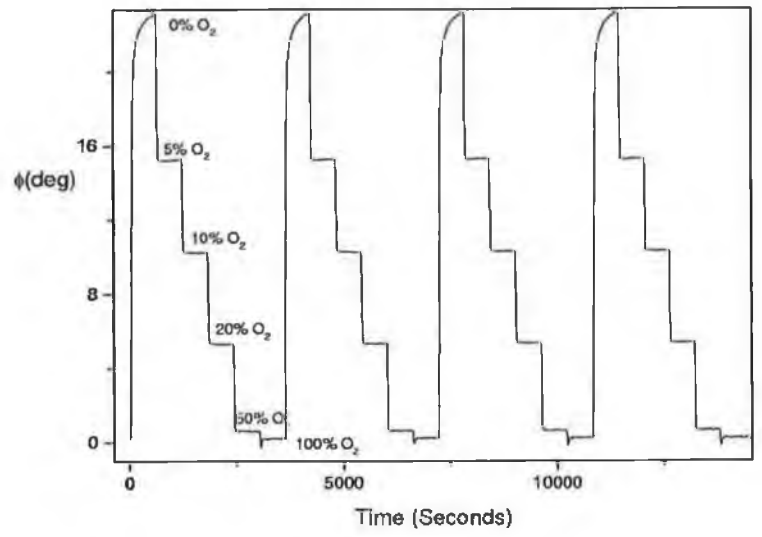


**Figure 7.5:** Response of $\phi$ v time for several cycles with a Ruthenium-doped film.

## 7.4 Modification of System for Porphyrin Oxygen Sensing

For oxygen sensing using PtOEPk-doped sensor films to be possible with the modular phase-fluorometric sensor system described here, various modifications had first to

be made. These modifications centred around two particular properties associated with the PtOEPk oxygen-sensitive complex. These properties were the fluorescence decay time of the PtOEPk complex and also the region of the electromagnetic(EM) spectrum in which it absorbs light and emits phosphorescence (see Sections 2.2 and 2.4).

Due to the longer decay time of PtOEPk compared to $[Ru(Ph_2phen)_3]^{2+}$ (60$\mu$s compared to 5$\mu$s), LEDs used to excite sensor films doped with PtEOPk must be modulated at a lower frequency according to Equation 2.5 in Section 2.6. In particular, the 20kHz modulation frequency used in the previous section for $[Ru(Ph_2phen)_3]^{2+}$-doped sensor films, must be reduced to a modulation frequency of 2.5kHz for PtOEPk-doped sensor films. The selection of the optimum modulation frequency for an oxygen-sensitive complex involves making a decision on whether the measurement range or the sensor sensitivity is the main concern. Figure 7.6 shows the variation of the $\phi$ value achieved for a range of modulation frequencies for a PtOEPk-doped sensor film. It also shows the variation of the intensity of the sine-wave modulated signal. As can be seen, the $\phi$ value increases with increasing frequency, but the signal level, as well as the SNR, decreases. The cross-over point is indicated on the plot, and both the $\phi$ and I values at this point are shown. A choice must be made on which property is of greater importance, however a useful guideline that can be used is the cross-over point of this plot. In this work this cross-over point is taken as the optimum modulation frequency and experiments were carried out using a modulation frequency very close to this value ($\sim$ 2.5kHz). A detailed discussion on the selection of the optimum modulation frequency for the $[Ru(Ph_2phen)_3]^{2+}$-doped sensing films can be found elsewhere[3, 4, 5].

Changing this modulation frequency was a simple task, as modulation frequency selection is one of the advantages of this modular system. It involved changing the combination of the dip-switches in the modulation circuit. However this longer decay time and thus lower modulation frequency created the need for more difficult modifications to be made to the sensing system.

In this portion of the work the fluorescence detection head shown in Figure 7.1 was used. This was instead of the DO probe head used for the $[Ru(Ph_2phen)_3]^{2+}$ sensor film experiments. The RC filtering circuitry contained within this detection head had been specifically designed for use at 20kHz, i.e. with $[Ru(Ph_2phen)_3]^{2+}$-doped sensor films. These RC filters had to be changed in order for signals modulated at 2.5kHz, that is the modulated phosphorescent light from the excited PtOEPk-

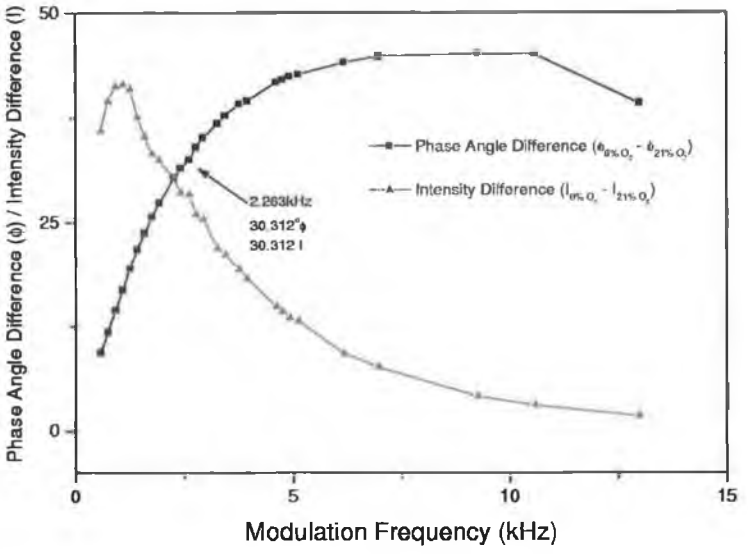


**Figure 7.6:** Selection of optimum frequency of modulation for work with PtOEPk complex.

doped films, be allowed to pass. This involved a calculation of the correct resistor and capacitor values to be made, and then for the existing resistors and capacitors to be replaced with the new calculated values, corrected for modulation at 2.5kHz.

The second property of the PtOEPk porphyrin complex that necessitated modifications to be made was its absorption and emission bands. As shown in Section 2.4 and in Figure 2.5, the PtOEPk complex absorbs in a different region of the EM spectrum than the $[Ru(Ph_2phen)_3]^{2+}$ complex. This required that the excitation LED used in the system be changed from a blue LED to a yellow LED. The yellow LED chosen was a Toshiba TLYH180P as used in the fibre-based sensor system described in Chapters 4 and 6. This yellow LED matched very well with the absorption band of the PtOEPk complex, as shown in Figure 2.5. The reference LED of the system was also changed from an amber LED to a red LED. This was done as the amber light($\lambda$ = 600nm) would not be passed through the optical filter used to pass the PtOEPk phosphorescent light of $\lambda$ = 751nm. The red LED used as a replacement had a wavelength of 700nm which was transmitted by the optical filter used(Schott Glass RG9 filter).

There were some problems encountered both in modifying this sensor system and also after the modifications had been completed. These problems affected the

operation of the sensor and are detailed in the following section.

## 7.5 Difficulties Encountered

There were several major difficulties encountered during this phase of testing and evaluating this modular phase-fluorometric sensor system. These were all associated with the switch over from testing $[Ru(Ph_2phen)_3]^{2+}$-doped sensor films to PtOEPk-doped sensor films. These problems and difficulties caused very little data to be recorded for PtOEPk-doped films tested with this system. These difficulties are summarised below.

One area that caused major difficulties was the changing of the RC filters in the circuitry of the fluorescence detection head. Eventhough the R and C values were calculated carefully, there was still some distortion of the signal passed through this RC filter. Several R values were tried in an attempt to optimise the passing of the 2.5kHz signals from the excited PtOEPk sensor films. This did not altogether remove the distortion in the detected signal. This meant that not all of the phosphorescent light from the excited PtOEPk complex, modulated at 2.5kHz, was being passed from the photodiode to the phase measuring module. The distortion of this photodiode signal provided incorrect $\phi$ values being recorded, which in turn led to false oxygen concentration readings.

There was however another factor that contributed to the distortion of the detected signal. The photodiode used in this fluorescent detection head had a slow response, and consequently the detected waveform was distorted. The DO probe head, described in Chapter 5, contained a different photodiode (S1223, Hamammatsu, UK) with a much faster response. This problem, combined with the RC filter difficulties encountered, increased the error in the $\phi$ value measured for an oxygen concentration level.

Another difficulty that was encountered during the testing of PtOEPk-doped sensor films with this modular phase-fluorometric sensor system involved the use of a different flow cell than that shown in Figure 7.2. It was necessary to use a different flow cell as the DO probe head was not used for testing the PtOEPk-doped films. Instead the photodiode-based fluorescence detection head was used, due to the ease with which the RC filters in this detection head could be accessed and modified. A diagram of the flow cell used here is shown in Figure 7.7.

In this new set-up the photodiode is further away from the sensing film than

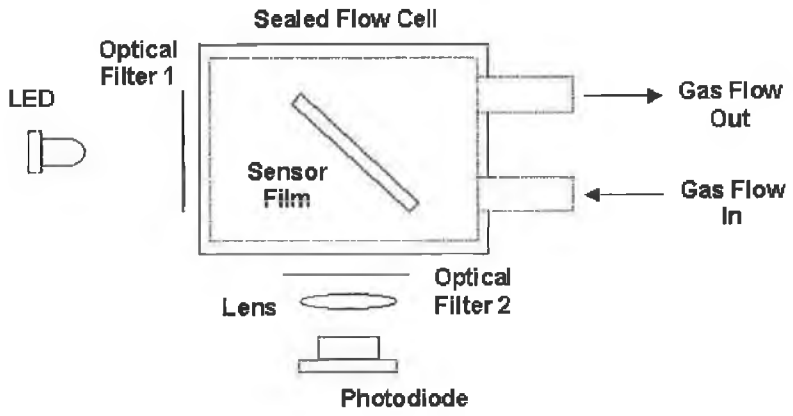


**Figure 7.7:** Square flow cell used for PtOEPk testing experiments.

in any of the other sensing set-ups described previously in this work. For this particular complex this is a problem, as is shown by the need for the fibre to be in close proximity to the sensor films in the fibre-based system described in Chapters 4 and 6. The light signal detected using the square flow cell set-up was quite small. When this problem was combined with the filter problems described above the errors in measuring $\phi$ were compounded.

One method that was investigated in an effort to increase the light signal detected by the photodiode during this PtOEPk phase of testing was an edge detection configuration. As is shown in Figure 7.8, when a planar substrate is coated with a fluorescent film on one side and illuminated by an excitation LED perpendicularly from the other, the fluorescence is coupled into the substrate. This fluorescence light is then transmitted down the waveguide and emerges at the end face. The angle of the emergence is consistent and is related to the refractive index values of the film and the substrate. This enables a photodiode to detect the fluorescent light reliably when placed at this exact angle. This, it was hoped, would increase the size of the detected light signal and allow a reliable value of $\phi$ to be recorded for these PtOEPk-based oxygen experiments. A more detailed description of this edge detection technique can be found elsewhere[6].

Although this technique did improve the size of the fluorescence signal detected, and the waveform could be seen to be quenched by the presence of oxygen, a reliable value for the phase-shift($\phi$) associated with the level of oxygen present could not be recorded. Throughout all this testing the high oxygen sensitivity of porphyrins proved a major impediment, as all the samples had to be degassed with 100%

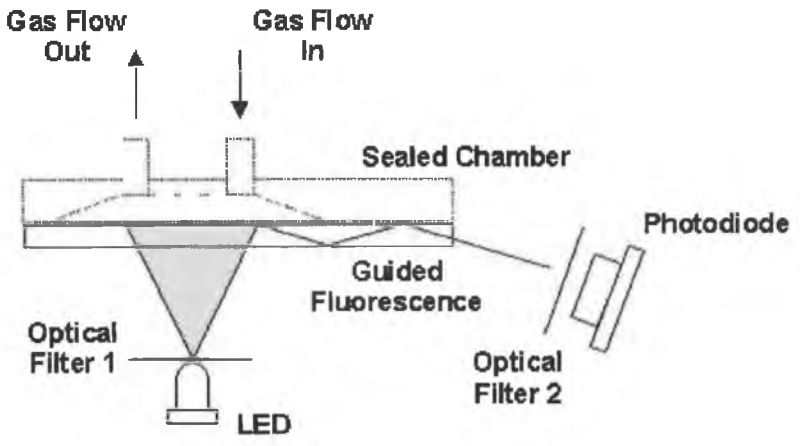


**Figure 7.8:** Edge detection set-up used for PtOEPk experiments.

nitrogen prior to testing as there was little or no fluorescence from the films at ambient oxygen concentrations.

At this point, time considerations dictated that further work on this system be continued by other researchers. It was clear that it was not straightforward to design a truly modular system, and that optimum sensor performance would only be obtained from a dedicated electronic design.

## 7.6 Summary

This chapter has introduced a modular phase-fluorometric sensor system designed in-house. The operation of this sensor system, which was based on a similar system described above in Chapters 4 and 5, has been detailed. Its performance as a sensor system has been evaluated. It was hoped that this system could be used to directly compare the performance of the two types of sensor films associated with this work, $[Ru(Ph_2phen)_3]^{2+}$-doped and PtOEPk-doped films, however several problems arose during the testing. These difficulties are introduced and detailed. Some solutions to these were investigated but with limited results. Ultimately it was not possible to test both film types using the same instrumentation. The modification of the modular system for porphyrin-based oxygen sensing is currently under way.

# Bibliography

[1] L. Polereky and J. Hamrle. Development of an optical sensor system based on fluorescence decay time measurement. *Unpublished*, 1995. School of Physical Sciences, Dublin City University.

[2] National Instruments. *LabVIEW User Manual.* 1998.

[3] A.K. McEvoy. *Development of an Optical Sol-Gel-Based Dissolved Oxygen Sensor.* PhD thesis, School of Physical Sciences, Dublin City University, 1995. Page 136.

[4] G. O'Keeffe, B.D. MacCraith, A.K. McEvoy, C.M. McDonagh, and J.F. McGlip. Development of a led-based phase-fluorimetric oxygen sensor using evanescent wave excitation of a sol-gel immobilized dye. *Sens and Act B*, 29:226–230, 1995.

[5] V.I. Ogurtsov and D.B. Papkovsky. Selection of modulation frequency of excitation for luminescence lifetime-based oxygen sensors. *Sens and Act B*, 51:377–381, 1998.

[6] J.F. Gouin, A. Doyle, and B.D. MacCraith. Fluorescence capture by planar waveguide as platform for optical sensors. *Electronic Letters*, 34:17, 1998.

# Chapter 8

# Concluding Remarks

## 8.1 Introduction

This chapter revisits the thesis objectives stated in Section 1.4 and evaluates how well these objectives have been achieved. The future development of aspects of the work are also discussed and, finally, conference presentations and publications arising from the work are detailed.

## 8.2 Achievement of Objectives

'**Objective** 1: To optimise and test a prototype dissolved oxygen sensor.

This objective has been achieved as detailed in Chapter 5.

**Objective** 2: To initiate field testing and make appropriate modifications/ improvements.

Initial field testing has been implemented with limited results. However, modifications and improvements have been made with a view to progressing to the next phase of testing.

**Objective** 3: To test and characterise a commercial porphyrin-based oxygen sensor and to investigate the use of porphyrin complexes in oxygen sensing, in particular to fabricate and evaluate porphyrin-doped sol-gel films.

The fibre probe was successfully tested and characterised. It was then used to characterise in-house fabricated porphyrin-doped sol-gel films. Three optimum

film formulations were identified with a view to using these in a new dedicated porphyrin probe based on the design of the probe head discussed in Chapter 5 and the electronic design discussed in Chapter 7.

**Objective** 4: To test a newly-designed modular phase-fluorometric system using both ruthenium complex-doped and porphyrin-doped films

This work was only partially successful. The modular electronic design was incorporated successfully into the ruthenium-complex oxygen probe and very good results were obtained for this system.

The work highlighted the difficulties involved in producing a truly modular, flexible sensor system. In particular, it is clear that the considerable differences in lifetime and in spectral properties for the two fluorophores used in this investigation would necessitate separate dedicated optical and electronic designs.

## 8.3 Future Developments

**Ruthenium-Complex-Based Sensor**

The electronics will be further optimised using the modular design discussed in Chapter 7 and the next phase of field testing will begin.

**Porphyrin-Based Sensor**

Further work is required to establish the feasibility of using sol-gel films instead of the well-established polymer films in these sensors. Whichever film is used, it is considered that using the probe configuration described in Chapter 5 in conjunction with an appropriately modified version of the electronics described in Chapter 7, will produce a very robust, sensitive oxygen sensor, suitable for many diverse applications.

## 8.4 Presentations and Publications Arising from the Work

1. Poster presentation: "Phase Fluorometric Dissolved Oxygen Sensor"; BOC Gases Poster Competition, March 2000, School of Physical Sciences, Dublin

City University.

2. Poster presentation: "Phase Fluorometric Dissolved Oxygen Sensor"; Institute of Physics of Ireland, Poster Presentation, Spring Weekend 200, Adare, Co. Limerick.

3. Poster presentation: "Phase Fluorometric Dissolved Oxygen Sensor"; Europtrode V, Poster Presentation, April 2000, Lyon, France.

4. Oral presentation: "Optical Dissolved Oxygen Sensor For Waste-Water Monitoring"; $11^{th}$ Irish Environmental Researchers Colloquium - Environ 2001, January 2001, Dublin City University.

5. Peer Reviewed Publication:
   "Phase Fluorometric Dissolved Oxygen Sensor"; McDonagh, C., Kolle, C., McEvoy, A.K., Dowling, D.L., Cafolla, A.A., Cullen, S.J., MacCraith, B.D.; Sensors and Actuators B, 2001, $74(1-3)$, $123-129$

# Appendix I

## Circuit Diagrams for Phase-Fluorometric Dissolved Oxygen Sensor

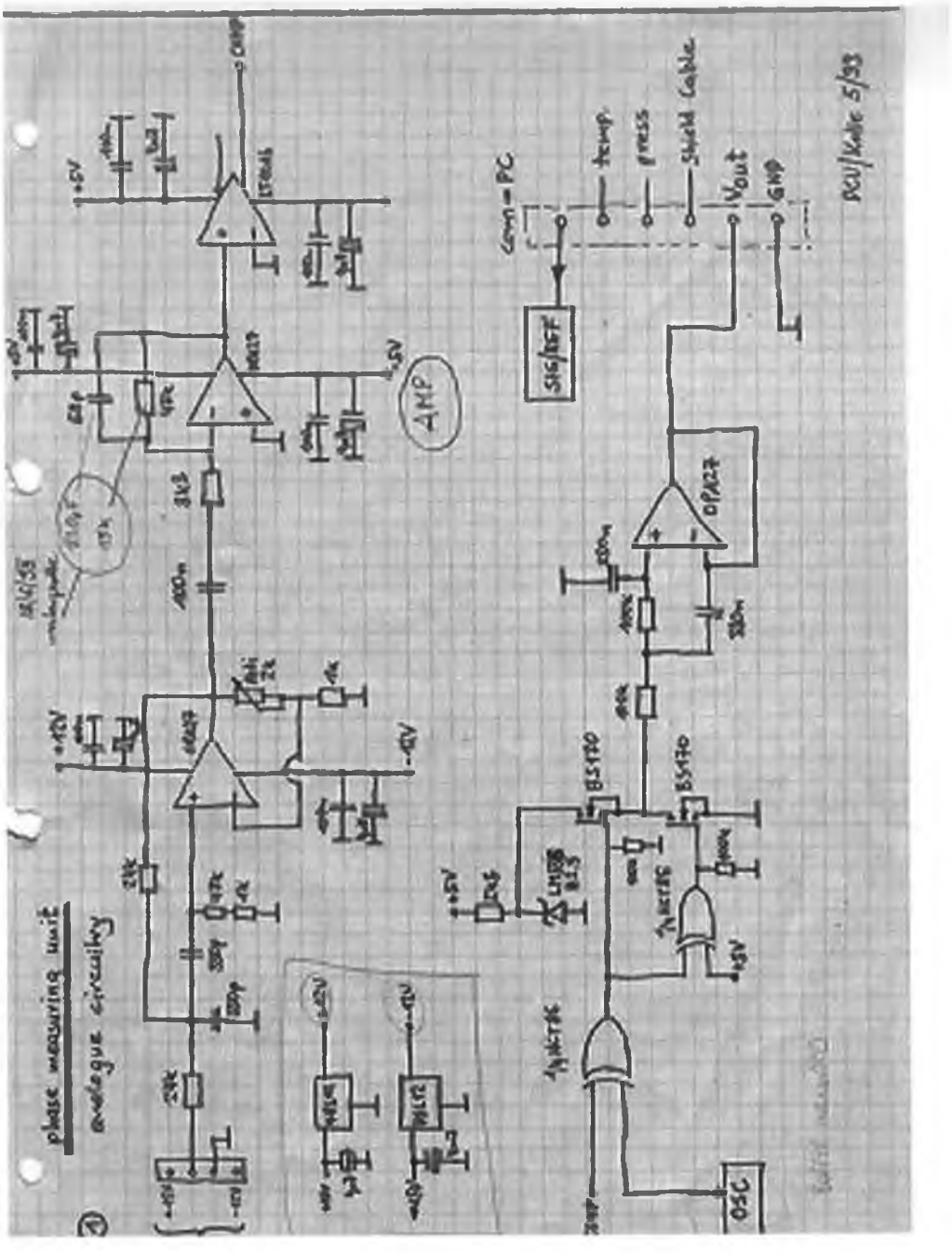


**Figure 1:** Schematic of Electronics of DO Sensor System

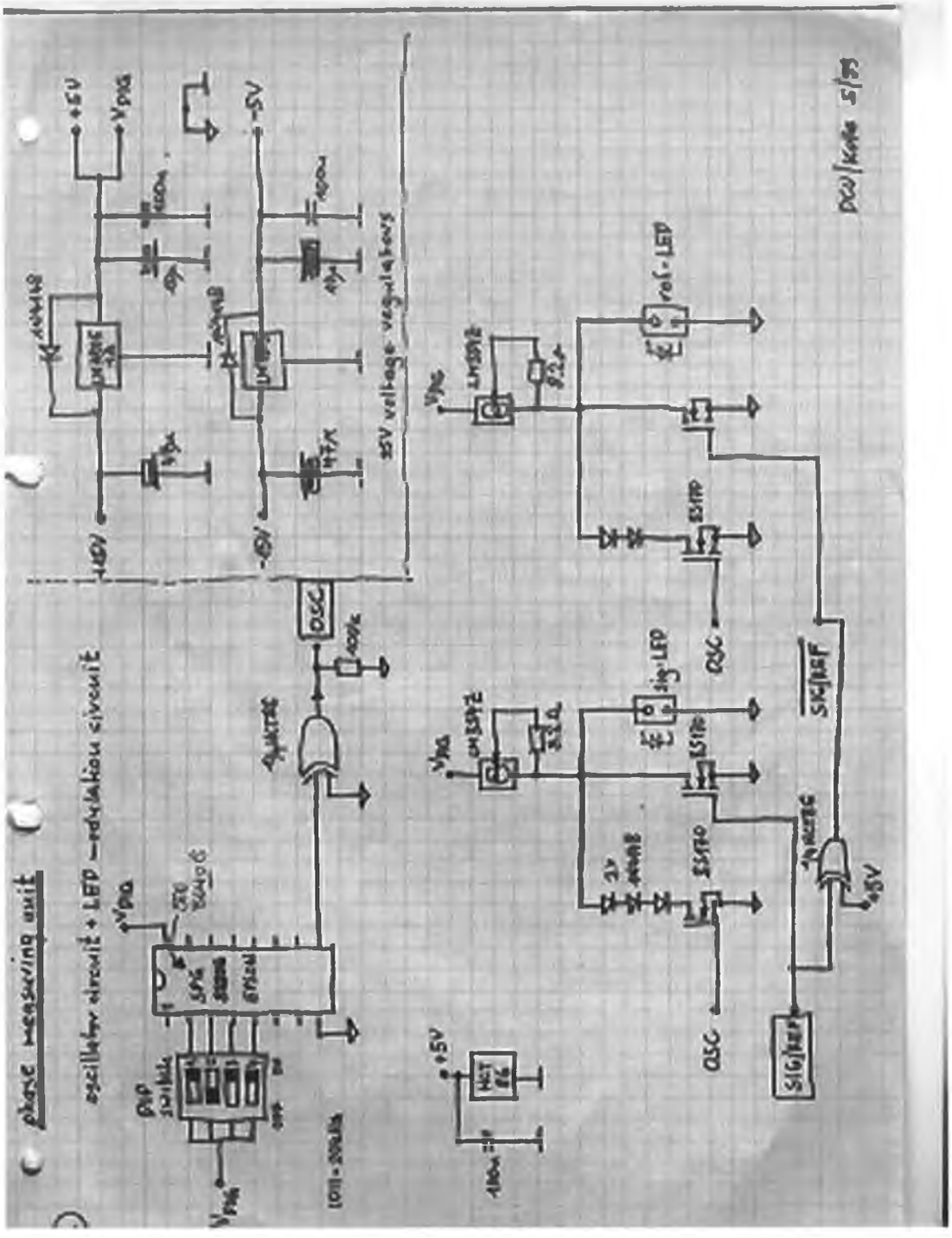


**Figure 2:** Schematic of Oscillator and LED Modulation Circuits for DO Sensor System

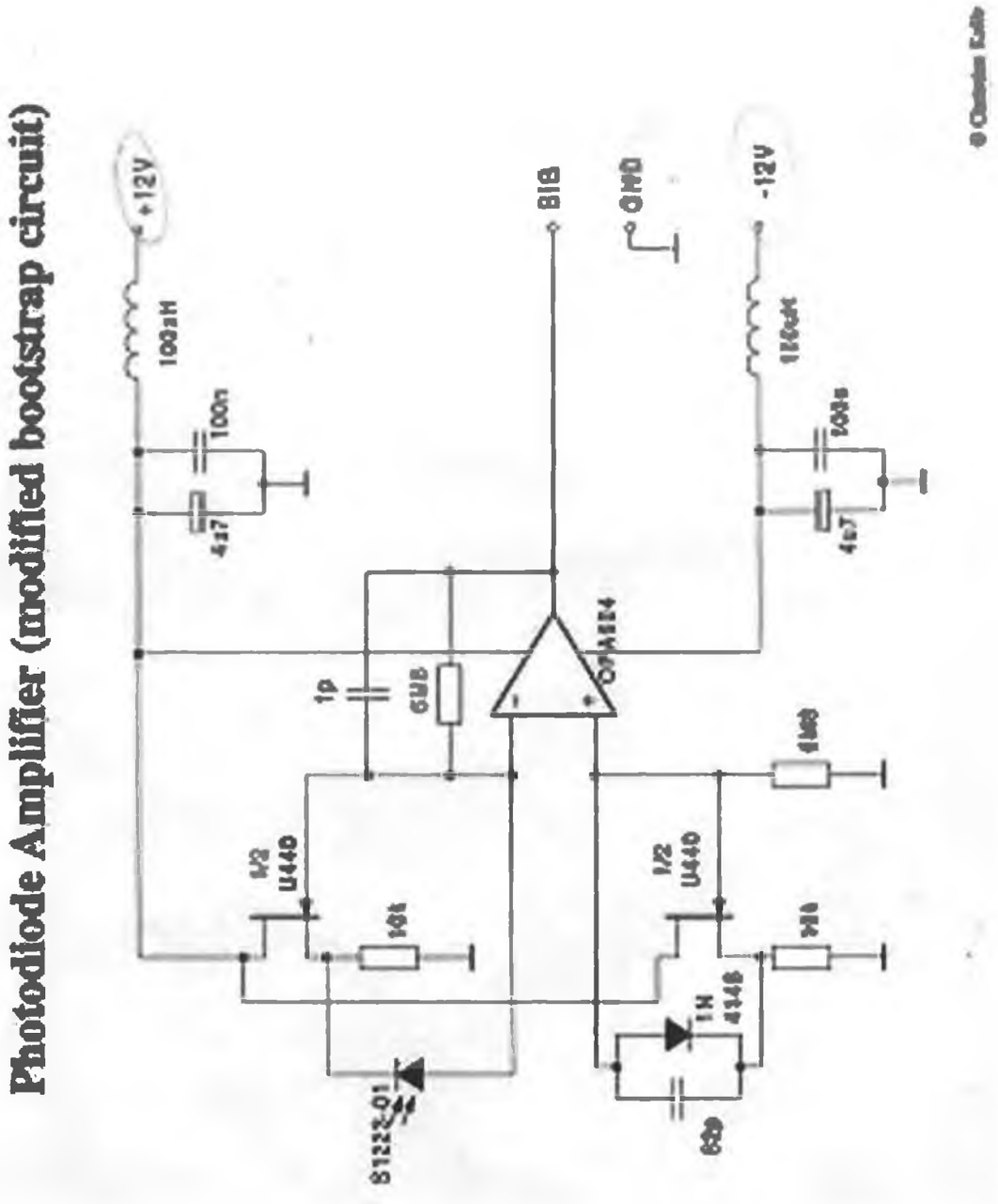


**Figure 3:** Schematic of Boot-Strapping Amplifier Circuit in DO Probe Head

# Appendix II

**DataAve.txt: Source Code for Microcal Origin Data Averaging Program**

```
getstring (Please enter the filename below) (filename) Filename;
open -w %B; //Opens the saved file
create.wks(A B C); //Opens a second wks.
copy Data1_A Data2_A; //and copies the relevent coloums
copy Data1_F Data2_B; //from the saved file, i.e. fie and O2
copy Data1_F Data2_C; //from the saved file, i.e. fie and O2
der Data2_C;
window -n plot[fievo2]; //Opens a graph window
layer.plotxy(Data2_A,Data2_B,200); //and plots fie v O2
layer -a; //showing the diff. cycles
window -n plot[dfievo2]; //Opens a graph window
layer.plotxy(Data2_A, Data2_C, 200); //and plots der(fie) v O2
layer -a; //showing the diff. cycles
create.wks(A B C); //Creates a third wks.
create.wks(A B C); //Creates a fourth wks.
create.wks(A B C); //Creates a fifth wks.
p=0; i=1; for(;p!=100;) //Loop reads in Oxygen concen. step
values {
    getn -s (Enter 100 to quit) p (Oxygen Concentration Values);
    Data3_A[i] = p;
    type (i);
    i + + ;
}
index=(i);
//index=;
t=0; getn -s (Temp in Degrees Celcius) t (Temperature of Water);
vapour=0; switch(t){
    case 5:
        vapour=8.726;
        break;
    case 10:
```

```
            vapour=12.281;
            break;
        case 15:
            vapour=17.056;
            break;
        case 20:
            vapour=23.388;
            break;
        case 25:
            vapour=31.69;
            break;
        case 30:
            vapour=42.455;
            break;
        default:
            type "You entered a temp that has not been set";
            break;
}
j=0; k=2; l=0; m=1; n=0; step=1; total=0; ptotal=0; diff=0;
result=0; pressure=0; var1=0; var2=0; r=0; value=0; taw0=0; taw=0;
top=0; btm0=0; btm=0;
for(step=1;step¡index;step | | ) {
    ptotal=0;
    presult=0;
    var1=0;
    var2=0;
    for(j=m;j¡k;j | | )
    {
        if(abs(Data2c[j]) < 0.015abs(Data2C[j | 200]) < 0.015)
        {
            k=j;
        }
        else
        {
            k=j | 2;
```

```
        }
//k=;
//j=;
    }
    m=j+1;
    for(l=j;l¡m;l++)
    {
        if(abs(Data2_c[l]) >= 0.015abs(Data2_C[l + 3]) >= 0.015)
        {
            m=l;
        }
        else
        {
            m=l+2;
        }
//m=;
//l=;
    }
    for(n=k;n¡=m;n++)
    {
        total+=Data2_B[n];
        ptotal+=Data1_D[n];
    }
    diff=m-k+1;
    result=total/diff;
    Data3¡step¦ = result;
    Data4¡step¦ = result;
    pressure=ptotal/diff;
    var1=(Data3¡step¦/100);
    var2=(pressure-vapour);
    presult=(var1*var2);
    Data4¡step¦ = presult;
    j=m;
    k=m+1;
    total=0;
```

```
}
copy Data4_B Data5_A; //from the saved file, i.e. fie and O2
data5_B[1]=1;
for(r=2;r¦index;r++) {
    top=125663.7061;
    btm0=tan(data3_b[1]);
    btm=tan(data3_b[r]);
    taw0=btm0/top;
    taw=btm/top;
    value=taw0/taw;
    data5_B[r]=value;
}
window -n plot[dfievo2]; //Opens a graph window
layer.plotxy(Data3_A,Data3_B,202); //and plots fie_averagev
layer -a; // concentration values.
window -n plot[dfievo2]; //Opens a graph window
layer.plotxy(Data4_B,Data4_A,202); //and plots fie_averagev
pressure layer -a; //compensated O2 values (hPa)
window -n plot[dfievo2]; //Opens a graph window
layer.plotxy(Data5_A,Data5_B,202); //and plots fie_averagev
Stern-Volmer layer -a; //data (taw0/taw)
//getstring (Please enter the save filename below) (filename) Save Filename;
[Data3!] wks.export.cntrl=2;
getfile *.*;
save -wh Data3 h:Probe%B; //Opens the saved file
```

# Appendix III

**Polyfit.for: The Source Code for Polyfit.exe**

```
PROGRAM POLYFIT
C Program to fit a ploynomial to a set of data
C TAC 3/10/99       REAL x(100),y(100),cof(15)
      CHARACTER fname*13
      Write(5,'(a)') ' Enter Data Filename: '
      read(5,*) fname
      write(5,'(a)') ' Enter degree of polymnomial: '
      read(5,*) ndeg
C read data from file
      open(unit = 1, file = fname, status = 'old',err = 100)
      do 10 i = 1,100
          read(1,*,end = 20) x(i),y(i)
10 continue
20 close(1)
      npts = i-1
      PRINT *, ' NPTS = ',npts
      call polcof(x,y,ndeg,cof)
      do 30 i = 1,ndeg
          print *,cof(i)
30 continue
C generate a fit file
      open(unit = 2, file = 'poly.fit',status = 'unknown')
      xs = (x(npts)-x(1))/100
      do 40 i = 1,100
          xpt = x(1)+(i-1)*xs
          call polint(x,y,npts,xpt,ypt,dy)
      write(2,*) xpt,ypt,dy
40 continue
      close(2)
      goto 150
100 write(5,'(a)') ' Unable to open file: ' 150 continue
```

```
      END

      SUBROUTINE POLCOF(XA,YA,N,COF)
      PARAMETER (NMAX=15)
      DIMENSION XA(N),YA(N),COF(N),X(NMAX),Y(NMAX)
      DO 11 J=1,N
          X(J)=XA(J)
          Y(J)=YA(J)
11 CONTINUE
      DO 14 J=1,N
          CALL POLINT(X,Y,N+1-J,0.,COF(J),DY)
          XMIN=1.E38
          K=0
          DO 12 I=1,N+1-J
              IF (ABS(X(I)).LT.XMIN)THEN
                  XMIN=ABS(X(I))
                  K=I
              ENDIF
              IF(X(I).NE.0.)Y(I)=(Y(I)-COF(J))/X(I)
12 CONTINUE
      IF (K.LT.N+1-J) THEN
          DO 13 I=K+1,N+1-J
              Y(I-1)=Y(I)
              X(I-1)=X(I)
13 CONTINUE
      ENDIF
14 CONTINUE
      RETURN      END

      SUBROUTINE POLINT(XA,YA,N,X,Y,DY)
      PARAMETER (NMAX=10)
      DIMENSION XA(N),YA(N),C(NMAX),D(NMAX)
      NS=1
      DIF=ABS(X-XA(1))
      DO 11 I=1,N
```

```
        DIFT=ABS(X-XA(I))
        IF (DIFT.LT.DIF) THEN
            NS=I
            DIF=DIFT
        ENDIF
        C(I)=YA(I)
        D(I)=YA(I)
11 CONTINUE
    Y=YA(NS)
    NS=NS-1
    DO 13 M=1,N-1
        DO 12 I=1,N-M
            HO=XA(I)-X
            HP=XA(I+M)-X
            W=C(I+1)-D(I)
            DEN=HO-HP
            IF(DEN.EQ.0.)PAUSE
            DEN=W/DEN
            D(I)=HP*DEN
            C(I)=HO*DEN
12 CONTINUE
    IF (2*NS.LT.N-M)THEN
        DY=C(NS+1)
    ELSE
        DY=D(NS)
        NS=NS-1
    ENDIF
    Y=Y+DY
13 CONTINUE
    RETURN
    END
```

**Poly.for: The Source Code for Poly.exe**

```
PROGRAM POLYFIT
C Program to fit a ploynomial to a set of data
C TAC 3/10/99
      REAL x(100),y(100),cof(15)
      CHARACTER fname*13,ans*1
      Write(5,'(a)') ' Enter Data Filename: '
      read(5,*) fname
      write(5,'(a)') ' Enter degree of polymnomial: '
      read(5,*) ndeg
      write(5,'(a)') ' Enter Scaling (Log, None, Sqrt), [L/N/S]: '
      read(5,'(a)') ans

C read data from file and transform x axis
      open(unit = 1, file = fname, status = 'old',err = 100)
      do 10 i = 1,100
            read(1,*,end = 20) x(i),y(i)
            if(ans .eq. 'L' .or. ans .eq. 'l') then
                  if (x(i) .ne. 0.0) then
                        x(i) = log(x(i))
                  endif
            endif
      if(ans .eq. 'S' .or. ans .eq. 's') then
            x(i) = sqrt(x(i))
      endif
      print *,i,x(i),y(i)
10 continue
20 close(1)
      npts = i-1
      PRINT *, ' NPTS = ',npts
      call polcof(x,y,ndeg,cof)
      do 30 i = 1,ndeg
            print *,cof(i)
30 continue
```

```
C generate a fit file
      open(unit = 2, file = 'poly.fit',status = 'unknown')
      xi = x(1)
      xf = x(npts)
      if(ans .eq. 'L' .or. ans .eq. 'l') then
           if(x(1) .eq. 0) then
                xi=0.0
           else
                xi=exp(x(1))
           endif
           xf=exp(x(npts))
      endif
      if(ans .eq. 'S' .or. ans .eq. 's') then
           if(x(1) .eq. 0) then
                xi=0.0
           else
                xi=x(1)*x(1)
           endif
           xf=x(npts)*x(npts)
      endif
      xs = (xf-xi)/100
      do 40 i = 1,100
           xpt = xi+(i-1)*xs
           if(ans .eq. 'L' .or. ans .eq. 'l') then
                if(xpt .ne.0.0) then
                     xpt = log(xpt)
                endif
           endif
      if(ans .eq. 'S' .or. ans .eq. 's') then
           xpt = sqrt(xpt)
      endif
           call polint(x,y,npts,xpt,ypt,dy)
      if(ans .eq. 'L' .or. ans .eq. 'l') then
           write(2,*) exp(xpt),ypt,dy
      endif
```

```
      if(ans .eq. 'S' .or. ans .eq. 's') then
          write(2,*) xpt*xpt,ypt,dy
      endif
      if(ans .eq. 'N' .or. ans .eq. 'n') then
          write(2,*) xpt,ypt,dy
      endif
40 continue
      close(2)
      goto 150
100 write(5,'(a)') ' Unable to open file: '
150 continue
      END
      SUBROUTINE POLCOF(XA,YA,N,COF)
      PARAMETER (NMAX=15)
      DIMENSION XA(N),YA(N),COF(N),X(NMAX),Y(NMAX)
      DO 11 J=1,N
          X(J)=XA(J)
          Y(J)=YA(J)
11 CONTINUE
      DO 14 J=1,N
          CALL POLINT(X,Y,N+1-J,0.,COF(J),DY)
          XMIN=1.E38
          K=0
          DO 12 I=1,N+1-J
              IF (ABS(X(I)).LT.XMIN)THEN
                  XMIN=ABS(X(I))
                  K=I
              ENDIF
              IF(X(I).NE.0.)Y(I)=(Y(I)-COF(J))/X(I)
12 CONTINUE
      IF (K.LT.N+1-J) THEN
          DO 13 I=K+1,N+1-J
              Y(I-1)=Y(I)
              X(I-1)=X(I)
13 CONTINUE
```

```
      ENDIF
14 CONTINUE
      RETURN
      END
      SUBROUTINE POLINT(XA,YA,N,X,Y,DY)
      PARAMETER (NMAX=100)
      DIMENSION XA(N),YA(N),C(NMAX),D(NMAX)
      NS=1
      DIF=ABS(X-XA(1))
      DO 11 I=1,N
        DIFT=ABS(X-XA(I))
        IF (DIFT.LT.DIF) THEN
          NS=I
          DIF=DIFT
        ENDIF
        C(I)=YA(I)
        D(I)=YA(I)
11 CONTINUE
      Y=YA(NS)
      NS=NS-1
      DO 13 M=1,N-1
        DO 12 I=1,N-M
          HO=XA(I)-X
          HP=XA(I+M)-X
          W=C(I+1)-D(I)
          DEN=HO-HP
          IF(DEN.EQ.0.)PAUSE
          DEN=W/DEN
          D(I)=HP*DEN
          C(I)=HO*DEN
12 CONTINUE
      IF (2*NS.LT.N-M)THEN
        DY=C(NS+1)
      ELSE
        DY=D(NS)
```

```
            NS=NS-1
         ENDIF
         Y=Y+DY
      13 CONTINUE
         RETURN
         END
```

# Appendix IV

**Cspl.for: Source Code for Cspl.exe**

```
program daragh
C
C test of Cubic Spline routine from numerical recipies
C
      real xa(100), ya(100), y2(100),x(1000), y(1000)
      real deriv(1000)
      character infile*12, ans*1, fout*12
C Read in Data File
1 Write(5,'(a)') ' Enter Filename: '
      read(5,*) infile
      open(unit = 1, file = infile, status = 'old',err = 100)
      do 10 i = 1,1000
          read(1,*, end = 11) xa(i), ya(i)
10 continue
11 close(1)
      npts = i-1
C Calculate derivative at beginning and end points
      yp1 = (ya(2)-ya(1))/(xa(2)-xa(1))
      yp2 = (ya(npts)-ya(npts-1))/(xa(npts)-xa(npts-1))
C Call Spline
      CALL SPLINE(xa,ya,npts,yp1,yp2,y2)
C Open output file
50 Write(5,'(a)') ' Enter Output Filename: '
      read(5,*) fout
      write(5,'(a)') ' Enter number of data points in output file: '
      read(5,*) nout
      open(unit = 2, file = fout, status = 'new',err = 110)
      xs = (xa(npts)-xa(1))/(nout-1)
C Call Splint to interploate
      do 20 i = 1, nout
          xpt = xa(1) + float(i-1)*xs
          call splint(xa,ya,y2,npts,xpt,ypt)
```

```
            write(5,*) i,xpt,ypt
            x(i) = xpt
            y(i) = ypt
20 continue
C Calculate the derivative of the data
      do 30 i = 2, nout
            deriv(i) = (y(i)-y(i-1))/(x(i)-x(i-1))
30 continue
      deriv(1) = deriv(2)
      do 40 i = 1, nout
            write(2,*) x(i),y(i),deriv(i)
40 continue
      close(2)
      goto 150
100 WRITE(5,'(A)') ' Unable to open file. Try again [Y/N] '
      read(5,'(a)') ans
      if (ans .eq. 'Y' .or. ans .eq. 'y') goto 1
      goto 150
110 WRITE(5,'(A)') ' Error in Output filename. Try again [Y/N] '
      read(5,'(a)') ans
      if (ans .eq. 'Y' .or. ans .eq. 'y') goto 50
150 continue
      end
C
C
C
      SUBROUTINE SPLINE(X,Y,N,YP1,YPN,Y2)
      PARAMETER (NMAX=100)
      DIMENSION X(N),Y(N),Y2(N),U(NMAX)
      IF (YP1.GT..99E30) THEN
            Y2(1)=0.
            U(1)=0.
      ELSE
            Y2(1)=-0.5
            U(1)=(3./(X(2)-X(1)))*((Y(2)-Y(1))/(X(2)-X(1))-YP1)
```

```
      ENDIF
      DO 11 I=2,N-1
          SIG=(X(I)-X(I-1))/(X(I+1)-X(I-1))
          P=SIG*Y2(I-1)+2.
          Y2(I)=(SIG-1.)/P
          U(I)=(6.*((Y(I+1)-Y(I))/(X(I+1)-X(I))-(Y(I)-Y(I-1))
     * /(X(I)-X(I-1)))/(X(I+1)-X(I-1))-SIG*U(I-1))/P
   11 CONTINUE
      IF (YPN.GT..99E30) THEN
          QN=0.
          UN=0.
      ELSE
          QN=0.5
          UN=(3./(X(N)-X(N-1)))*(YPN-(Y(N)-Y(N-1))/(X(N)-X(N-1)))
      ENDIF
      Y2(N)=(UN-QN*U(N-1))/(QN*Y2(N-1)+1.)
      DO 12 K=N-1,1,-1
          Y2(K)=Y2(K)*Y2(K+1)+U(K)
   12 CONTINUE
      RETURN
      END
C
C
C
      SUBROUTINE SPLINT(XA,YA,Y2A,N,X,Y)
      DIMENSION XA(N),YA(N),Y2A(N)
      KLO=1
      KHI=N
1       IF (KHI-KLO.GT.1) THEN
          K=(KHI+KLO)/2
      IF(XA(K).GT.X)THEN
          KHI=K       ELSE
          KLO=K
      ENDIF
      GOTO 1
```

```
      ENDIF
      H=XA(KHI)-XA(KLO)
      IF (H.EQ.0.) PAUSE 'Bad XA input.'
      A=(XA(KHI)-X)/H
      B=(X-XA(KLO))/H
      Y=A*YA(KLO)+B*YA(KHI)+
     * ((A**3-A)*Y2A(KLO)+(B**3-B)*Y2A(KHI))*(H**2)/6.
      RETURN
      END
```

**Cspl2d.for: Source Code for Cspl2d.exe**

```
program daragh
C
C test of Cubic Spline routine from numerical recipies
C       real conc(100), ph(100), y2(100), temp(100), conct(100)
      character*12 infile(100), ftmp*12
C Read in Parameter File
      CALL GETPARM(infile,nfiles,temp)
      ntemp = nfiles
C Enter the required phase and temperature
      Write(5,'(a)') ' Enter Required Phase: '
      read(5,*) phase
      Write(5,'(a)') ' Enter Required Temperature: '
      read(5,*) tmpreq
C Loop through each conc vs phase file and get the conc at
C the required phase in each temp file
      do 20 j = 1,nfiles
          ftmp = infile(j)
          open(unit = 1, file = ftmp, status = 'old' ,err = 100)
          do 10 i = 1,1000
              read(1,*, end = 11) conc(i), ph(i)
c               print *,i,conc(i),ph(i)
10 continue
```

```
11 close(1)
      npts = i-1
C Sort data so phase is in ascending order
      call sort2(npts,ph,conc)
C Check if phase is inside or outside calibration curve range
      if((phase .lt. ph(1)) .or. (phase .gt. ph(npts))) then
          write(5,'(a,2x,i4)')
*           ' Phase is outside calibration range in cal-file',j
      endif
C This section is just a test
c       do 211 k = 1,npts
c           print *,k,conc(k),ph(k)
c211 continue
C Calculate derivative at beginning and end points
      conc1 = (conc(2)-conc(1))/(ph(2)-ph(1))
      conc2 = (conc(npts)-conc(npts-1))/(ph(npts)-ph(npts-1))
C Call Spline
      CALL SPLINE(ph,conc,npts,conc1,conc2,y2)
C Call Splint to interploate the conc at the required phase
      call splint(ph,conc,y2,npts,phase,concph)
      conct(j) = concph
c           print *, 'The conc at ',phase,' in file ',j,' is ',concph
20 continue
C Now interpolate in the temperature direction
      if((tmpreq .lt. temp(1)) .or. (tmpreq .gt. temp(ntemp))) then
      write(5,'(a)') 'Temperature is outside calibration range'
      endif
C Calculate derivative at beginning and end points
      conc1=(conct(2)-conct(1))/(temp(2)-temp(1))
      conc2=(conct(ntemp)-conct(ntemp-1))/(temp(ntemp)-temp(ntemp-1))
C Call Spline
      CALL SPLINE(temp,conct,ntemp,conc1,conc2,y2)
C Call Splint to interploate the conc at the required phase
      call splint(temp,conct,y2,ntemp,tmpreq,conctemp)
      print *, 'The conc at temperature = ',tmpreq
```

```
      print *, ' and phase = ',phase,' is ',conctemp
      goto 150
100 WRITE(5,'(A)') ' Unable to open one of the input file '
      WRITE(5,'(a)') ' Check names in Parameter file: '
      stop
150 continue
      end
C
C
C
      SUBROUTINE GETPARM(infile,nfiles,temp)
      real temp(100)
      character*12 infile(100), pfile
      character ans*1
1 Write(5,'(a)') ' Enter Parameter Filename: '
      read(5,*) pfile
      open(unit = 2, file = pfile, status = 'old',err = 100)
      read(2,*) nfiles
      Write(5,*) ' Number of Data FIles = ',nfiles
      do 10 i = 1,nfiles
          read(2,*) infile(i),temp(i)
          write(5,*) i,' ',infile(i),temp(i)
10 continue
      close(2)
      RETURN
100 WRITE(5,'(A)') ' Unable to open file. Try again [Y/N] '
      read(5,'(a)') ans
      if (ans .eq. 'Y' .or. ans .eq. 'y') goto 1
      stop
      END
C
C
C
      SUBROUTINE SPLINE(X,Y,N,YP1,YPN,Y2)
      PARAMETER (NMAX=100)
```

```
      DIMENSION X(N),Y(N),Y2(N),U(NMAX)
      IF (YP1.GT..99E30) THEN
          Y2(1)=0.
          U(1)=0.
      ELSE
          Y2(1)=-0.5
      U(1)=(3./(X(2)-X(1)))*((Y(2)-Y(1))/(X(2)-X(1))-YP1)
      ENDIF
      DO 11 I=2,N-1
          SIG=(X(I)-X(I-1))/(X(I+1)-X(I-1))
          P=SIG*Y2(I-1)+2.
          Y2(I)=(SIG-1.)/P
          U(I)=(6.*((Y(I+1)-Y(I))/(X(I+1)-X(I))-(Y(I)-Y(I-1))
     * /(X(I)-X(I-1)))/(X(I+1)-X(I-1))-SIG*U(I-1))/P
   11 CONTINUE
      IF (YPN.GT..99E30) THEN
          QN=0.
          UN=0.
      ELSE
          QN=0.5
          UN=(3./(X(N)-X(N-1)))*(YPN-(Y(N)-Y(N-1))/(X(N)-X(N-1)))
      ENDIF
      Y2(N)=(UN-QN*U(N-1))/(QN*Y2(N-1)+1.)
      DO 12 K=N-1,1,-1
          Y2(K)=Y2(K)*Y2(K+1)+U(K)
   12 CONTINUE
      RETURN
      END
C
C
C
      SUBROUTINE SPLINT(XA,YA,Y2A,N,X,Y)
      DIMENSION XA(N),YA(N),Y2A(N)
      KLO=1
      KHI=N
```

```
1 IF (KHI-KLO.GT.1) THEN
        K=(KHI+KLO)/2
        IF(XA(K).GT.X)THEN
            KHI=K
        ELSE
            KLO=K
        ENDIF
        GOTO 1
    ENDIF
    H=XA(KHI)-XA(KLO)
    IF (H.EQ.0.) PAUSE 'Bad XA input.'
    A=(XA(KHI)-X)/H
    B=(X-XA(KLO))/H
    Y=A*YA(KLO)+B*YA(KHI)+
* ((A**3-A)*Y2A(KLO)+(B**3-B)*Y2A(KHI))*(H**2)/6.
    RETURN
    END
c
c
c
    SUBROUTINE SORT2(N,RA,RB)
    DIMENSION RA(N),RB(N)
    L=N/2+1
    IR=N
10 CONTINUE
    IF(L.GT.1)THEN
        L=L-1
        RRA=RA(L)
        RRB=RB(L)
    ELSE
        RRA=RA(IR)
        RRB=RB(IR)
        RA(IR)=RA(1)
        RB(IR)=RB(1)
        IR=IR-1
```

REFERENC

```
            IF(IR.EQ.1)THEN
                RA(1)=RRA
                RB(1)=RRB
                RETURN
            ENDIF
        ENDIF
        I=L
        J=L+L
20 IF(J.LE.IR)THEN
            IF(J.LT.IR)THEN
                IF(RA(J).LT.RA(J+1))J=J+1
                ENDIF
            IF(RRA.LT.RA(J))THEN
                RA(I)=RA(J)
                RB(I)=RB(J)
                I=J
                J=J+J
            ELSE
                J=IR+1
            ENDIF
        GO TO 20
        ENDIF
        RA(I)=RRA
        RB(I)=RRB
        GO TO 10
        END
```